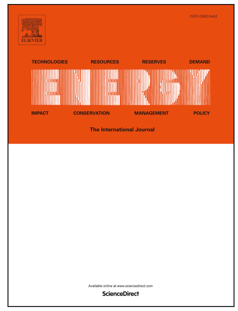

Modelling of organic Rankine cycle power systems in off-design conditions: An experimentally-validated comparative study

Rémi Dickes, Olivier Dumont, Rémi Daccord, Sylvain Quoilin, Vincent Lemort

PII: S0360-5442(17)30137-8

DOI: 10.1016/j.energy.2017.01.130

Reference: EGY 10265

To appear in: *Energy*

Received Date: 29 August 2016

Revised Date: 5 December 2016

Accepted Date: 25 January 2017

Modelling of organic Rankine cycle power systems in off-design conditions: an experimentally-validated comparative study

Rémi Dickes[a,*], Olivier Dumont[a], Rémi Daccord[b], Sylvain Quoilin[a], Vincent Lemort[a]

[a] *Thermodynamics Laboratory, Faculty of Applied Sciences, University of Liège Allée de la Découverte 17, B-4000, Liège, Belgium*
[b] *Exoès, 6 Avenue de la Grande Lande, F-33170, Gradignan, France*

Abstract

Because of environmental issues and the depletion of fossil fuels, the world energy sector is undergoing many changes toward increased sustainability. Among the many fields of research and development, power generation from low-grade heat sources is gaining interest and the organic Rankine cycle (ORC) is seen as one of the most promising technologies for such applications. In this paper, it is proposed to perform an experimentally-validated comparison of different modelling methods for the off-design simulation of ORC-based power systems. To this end, three types of modelling paradigms (namely a constant-efficiency method, a polynomial-based method and a semi-empirical method) are compared both in terms of their fitting and extrapolation capabilities. Post-processed measurements gathered on two experimental ORC facilities are used as reference for the models calibration and evaluation. The study is first applied at a component level (i.e. each component is analysed individually) and then extended to the characterization of the entire organic Rankine cycle power systems. Benefits and limitations of each modelling method are discussed. The results show that semi-empirical models are the most reliable for simulating the

*Corresponding author
Email addresses: rdickes@ulg.ac.be (Rémi Dickes), olivier.dumont@ulg.ac.be (Olivier Dumont), remi.daccord@exoes.com (Rémi Daccord), squoilin@ulg.ac.be (Sylvain Quoilin), vincent.lemort@ulg.ac.be (Vincent Lemort)

off-design working conditions of ORC systems, while constant-efficiency and polynomial-based models are both demonstrating lack of accuracy and/or robustness.

Keywords: Organic Rankine Cycle, modelling, off-design, experimental data, simulation

1. Introduction

Among the many fields of research and development toward increased sustainability, power generation from low-grade heat sources (i.e. below 200°C) is gaining interest because of its enormous worldwide power potential. In this context, the Organic Rankine Cycle (ORC) is acknowledged as one of the most suitable technologies for valorizing low-grade heat into electricity or mechanical power [1]. The working principle of an ORC is identical with that of a conventional steam Rankine engine: it constitutes a closed-loop thermodynamic cycle into which a working fluid undergoes a series of processes (i.e. compression, evaporation, expansion and condensation) aiming to partially convert thermal power from a heat source into mechanical power. The distinction is related to the nature of the working fluid: instead of using water like in a conventional steam Rankine cycle, ORC systems employ organic compounds which are characterized by lower boiling points and higher molecular mass. By substituting water for such organic fluids, it is possible to perform efficiently the Rankine cycle at low power capacities and using heat from low-grade thermal sources [1].

The technology of the ORC is rather old and first experimental facilities date from the late nineteenth century [2, 3]. Nowadays, the total power capacity installed worldwide is estimated at 2 GWe [4] and ORC-based power systems have continuously been gaining in interest for more than a decade. As a figure of merit, the number of papers yearly published about organic Rankine cycles is illustrated in Figure 1. Most of these scientific works focus on

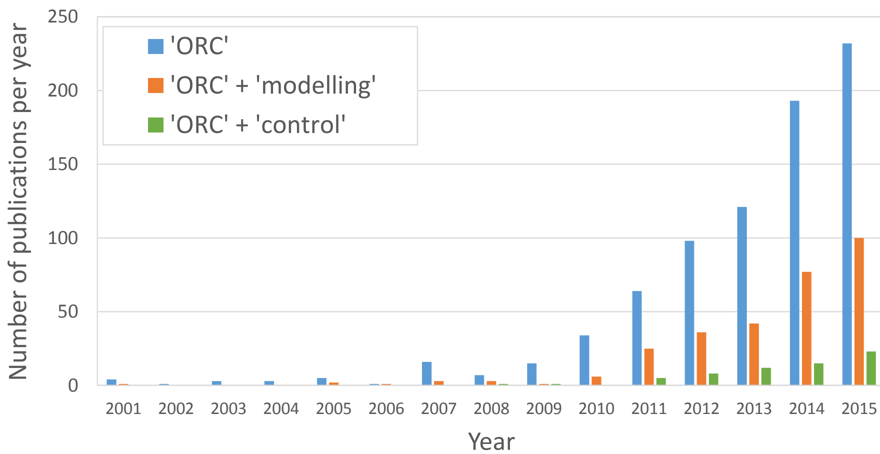

Figure 1: Yearly number of publications related to ORC systems from 2001 to 2015 (source: advanced search with different keywords in ScienceDirect)

design optimization, proper fluid selection, exergy/energy analyses and various techno-economic studies. However, a common feature of ORC-based systems is the versatile nature of the operating conditions. In most of the fields of application (e.g. solar thermal power, combined heat and power, geothermal or waste heat recovery), the heat source (and eventually the heat sink) fluctuates in time and the machine must adapt its working regime to ensure an optimal system operation. Despite of its importance, the number of papers related to control aspects and off-design performance of ORC systems is comparatively low.

A few steady-state performance analyses have been published for different ORC architectures and applications. For instance, Gurgenci [5] proposed a simple semi-analytical model to assess the performance of ORC-based power plants. The model aimed to easily derive the off-design behaviour of any ORC system based on its design operating conditions. The case of a 150 kWe solar pond power plant was studied as an example and Gurgenci discussed the dependence of the system efficiency in function of the turbine load and the hot and cold fluids supply temperatures. Another solar-driven ORC power plant was investigated in off-design operation by Wang et al. [6]. The system consisted of a 250 kWe ORC module (R245fa as working fluid) coupled to a thermal energy storage and compound parabolic collectors. The off-design performance of the whole power plant was assessed under variations in the ambient temperature and the heat source mass flow rate. Similarly, Calise et al. [7] studied a 230 kWe recuperative ORC power unit (n-butane as working fluid) coupled with solar parabolic trough collectors. After optimally sizing the different shell-and-tube heat exchangers (i.e. the recuperator, economizer, evaporator and superheater), the authors evaluated the ORC off-design behaviour while varying the thermal heat source both in terms of mass flow rate and supply temperature. In the same power scale, Fu et al. [8] performed a theoretical study on a 250 kWe ORC using R245fa as working fluid. Only the influence of the heat source mass flow rate on the power plant performance was considered. The ORC was controlled following a sliding pressure strategy: the evaporation pressure was controlled to ensure the working fluid to reach saturated liquid and vapour states at the outlet of the preheater and the evaporator respectively. Hu et al. [9] proposed a more physical analysis and investigated three control schemes to operate a 70 kWe geothermal ORC unit, namely a constant-pressure strategy, a sliding-pressure strategy and optimal-pressure strategy. The system featured a radial inflow turbine, plate heat exchangers and used R245fa as working fluid. Both the refrigerant mass flow rate and variable inlet guide vanes were used to adapt the power plant behaviour in function of the operating conditions (variation of the heat source supply temperature and mass flow rate). Manente et al. [10] studied a much larger geothermal power plant (> 5 MWe) and performed a constrained optimization to maximize the system net power output. Both R134a and Isobutane were considered as working fluid and three variables were used to control the plant behaviour, namely the pump speed, the cooling air mass flow rate in the condenser and the turbine capacity factor. Both variations of the ambiance and heat source supply temperature were considered in the study. Sun and Li [11] also analysed the off-design control of a 5 MWe ORC unit. They demonstrated that the relationships between controlled variables (optimal working fluid and air mass flow rates) and external perturbations (heat source and ambient temperatures) are near linear function for maximizing the system net power generation and quadratic function for maximizing the system thermal efficiency. Finally, Quoilin [12] analysed the off-design performance of a micro-scale 1.5 kWe ORC prototype. The system consisted of plate heat exchangers, a scroll expander and employed R123 as working fluid. A control of the pump and the expander speeds was proposed to maximize the ORC thermal efficiency. All the aforementioned studies were performed in steady-state conditions. However, the transients affecting the boundary conditions of the ORCs are often faster than the response time of the system. In such case, proper control investigations and off-design analyses require to account for the dynamic effects induced by mass and energy accumulations in the various ORC components. Such dynamic performance assessment and control studies can also be found in the scientific literature, see for example [13, 14, 15, 16, 17, 18, 19, 20].

The works presented here above have one feature in common: they all used mathematical models to predict the behaviour of the ORCs and their components in off-design conditions. Indeed, making measurements on existing power units is costly and time-consuming, and very few papers published experimental data characterizing ORC systems over their complete operating ranges (see one example in [21]). In almost every case, the experimental data (if there is any) gathered on the facility only covers a narrow range of the feasible operating conditions and they are not sufficient for a global empirical characterization of the system. Extrapolating the ORC performance in unknown working conditions can be performed by means of off-design modelling tools. As shown in the aforementioned papers, there is a wide variety of modelling paradigms to estimate the components state in an ORC system, ranging from the simplest method (e.g. to assume constant efficiencies for characterizing a turbine) to the most complex one (e.g. CFD modelling of the same turbine). Each modelling method differs from the others in terms of complexity, accuracy, computational speed, calibration effort and domain of validity. Commonly, the most accurate and reliable models implement detailed physics-based equations which leads to high simulation time. However, the calculation speed is a key parameter to maximize in the case of computationally-intensive simulations like control optimization. A common way to meet this requirement is to decrease the models complexity, resulting often in a loss of accuracy. Therefore, there is a trade-off between modelling complexity and simulation accuracy which deserves being studied.

In this paper, it is proposed to perform an experimentally-validated analysis of different modelling methods for the simulation of ORC systems in off-design conditions. More specifically, this work aims at comparing three common modelling paradigms (presented in section 3) both in terms of their fitting and extrapolation abilities. Measurements on two experimental ORC test rigs are used as reference (for the models calibration and evaluation) and the database are presented in section 2. The study is first applied to the components level (i.e. each component is analysed individually) in section 4 and then extended to the characterization of the entire ORC systems in section 5. A particular attention is given to the complete ORC system modelling. In most of the works presented in the state of the art here above, the off-design ORC models rely on several intrinsic user-defined assumptions like imposed superheating, refrigerant mass flow rate, condensing or evaporating pressure. In this work, except for the condenser subcooling which needs to be specified (the ORC model is not charge sensitive), the ORC model is developed so that the system performance is deduced by only taking as inputs the boundary conditions of the system.

The modelling tools and source codes developed to perform this work can be found in the open-source *ORCmKit* modelling library [22] and thermo-physical properties of the fluids are computed with CoolProp [23].

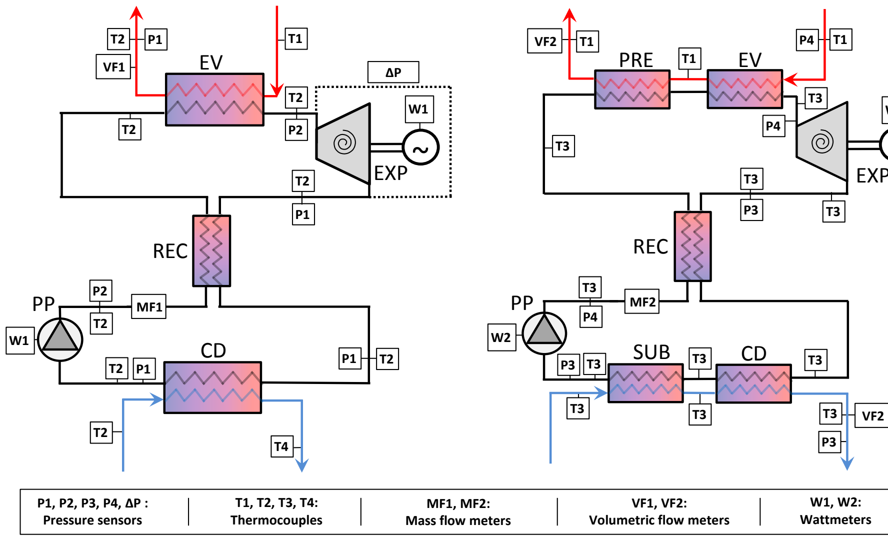

Figure 2: Experimental facilities ORC_1 (left) and ORC_2 (right) - details about the sensors are provided in Table 1.

2. Test rigs and experimental database

In this work, two experimental facilities (depicted in Figure 2) are used as case study for the derivation of different kinds of models. The following section describes the two test rigs and the experimental campaigns performed to characterize the systems performance.

2.1. Test rigs description

The first system considered is the *Sun2Power* ORC module developed by the University of Liège for a solar thermal application [24, 25]. It is a 3 kWe recuperative organic Rankine cycle using R245fa as working fluid. It is constituted of scroll expander with variable rotational speed and a diaphragm pump. Both the recuperator and the evaporator are brazed plate heat exchangers (protected with a 3cm-thick thermal insulation), while an air-cooled fin coil heat exchanger is used for the condenser. Variable-frequency drives are used to control both the rotational speeds of the pump and the condenser fan. On the other hand, the

Table 1: Sensors properties (FS = full scale)

Sensor type	Range	Absolute accuracy
T1 (thermocouple type T)	$[133°C \dots 350°C]$	$1°C$
T2 (thermocouple type T)	$[-40°C \dots 133°C]$	$1°C$
T3 (thermocouple type T)	$[-40°C \dots 133°C]$	$0.75°C$
T4 (thermocouple type T)	$[-40°C \dots 133°C]$	$5°C$
P1 (absolute pressure)	$[0bar \dots 10bar]$	$1\% \cdot FS$
P2 (absolute pressure)	$[0bar \dots 40bar]$	$1\% \cdot FS$
P3 (absolute pressure)	$[0bar \dots 10bar]$	$0.75\% \cdot FS$
P4 (absolute pressure)	$[0bar \dots 40bar]$	$0.75\% \cdot FS$
ΔP (differentiate pressure)	$[0bar \dots 20bar]$	$1\% \cdot FS$
MF1 (coriolis flow meter)	$[0kg/min \dots 20kg/min]$	$0.15\% \cdot FS$
MF2 (coriolis flow meter)	$[0.5kg/min \dots 50kg/min]$	$0.25\% \cdot FS$
VF1 (volumetric flow meter)	$[0.3m^3/h \dots 30m^3/h]$	$5\% \cdot FS$
VF2 (volumetric flow meter)	$[0.1m^3/h \dots 12m^3/h]$	$0.5\% \cdot FS$
W1 (wattmeter)	$[0W \dots 2000W]$	$1\% \cdot FS$
W2 (wattmeter)	$[0W \dots 10000W]$	$0.75\% \cdot FS$

expander rotational speed is controlled by means of a variable electrical load. The second system investigated is the *Microsol* 10 kWe ORC unit developed by EXOES and integrated into a concentrated solar power (CSP) plant [26]. It is also a recuperative cycle running R245fa as working fluid and the same pump technology is used. A scroll expander (grid-connected with constant rotational speed) performs the expansion and two additional heat exchangers are installed to ensure the fluid preheating and subcooling (in total, the second system includes five thermally-insulated brazed plate heat exchangers).

In addition to the cycle components, both test rigs are fully instrumented for measuring the experimental performance of each subsystem. As illustrated in Figure 2, thermocouples, pressure sensors, flow meters and electric power meters are installed along the plants to ensure a proper characterization of the systems. Technical details regarding these sensors are given in Table1. For the sake of simplicity, the *Sun2Power* and the *Microsol* experimental facilities will be further referred to as ORC_1 and ORC_2 and Table 2 summarizes their main

Table 2: Main features of the two experimental facilities

Properties	Facility ORC_1	Facility ORC_2
Nominal net power output	3 kWe	10 kWe
Working fluid	R245fa	R245fa
Heat source fluid	Thermal oil (Pirobloc HTF-Basic)	Pressurized water ($\sim$ 10 bar)
Heat sink fluid	Ambient air	Water-glycol mixture (30% vol.)
Expander	Scroll expander (variable speed)	Scroll expander (constant speed)
Pump	Diaphragm pump (variable speed)	Diaphragm pump (variable speed)
Condenser	Fin coil HEX (fan with variable speed)	Brazed plate HEX
Subcooler	n.a.	Brazed plate HEX
Evaporator	Brazed plate HEX	Brazed plate HEX
Preheater	n.a.	Brazed plate HEX
Recuperator	Brazed plate HEX	Brazed plate HEX

characteristics.

2.2. Database description

For both test rigs, experiments are conducted to characterize the systems performance under various steady-state operating conditions. In these experimental campaigns, the ORC systems are not operated in accordance with any dedicated control strategy. Instead, the test rigs are evaluated over extended ranges of conditions (including non-optimal points) in order to properly characterize their behaviours in off-design and part-load operations. Quasi steady-state performance points are obtained by averaging the measurements over 2-minute periods in stabilized regimes (i.e. conditions for which the deviations in all the temperatures are lower than $1°C$, with non-sliding pressures and with constant mass flow rates). Two initial datasets of 57 and 59 experimental points are collected for the facilities ORC_1 and ORC_2, respectively. Because the measured numerical values are subject to different uncertainties, possible errors or sensor malfunction, a thorough data post-treatment is performed. In a first step, outliers resulting of sensor malfunction or noise in the acquisition chain are detected and discarded from the database. For these points, the measurements of one or several sensors are out of any confidence interval and do not represent the physics of the machine. These outliers are automatically identified using the open-source *GPExp* library. Based on Gaussian processes theory, this numerical tool proposes a methodology for quality assessment of steady-state experimental data, as extensively described in [27]. Once the outliers are identified and discarded from the original datasets, a second post-process is applied to the remaining measurements. Because the sensors present a limited accuracy (in the form of noise or of a systematic error), any measurement gathered during the experimental campaign is contaminated by an unknown error. Although limited locally, the propagation of these measurements errors results in systems conditions that violate theoretical postulates onto which the models are developed. For instance, the heat transfer rate experimentally evaluated on the cold side of a well-insulated heat exchanger almost never match the heat transfer evaluated on the hot side (cfr. Figure 3). However, by accounting for the sensors inaccuracy, an ideal heat balance can be retrieved, as it is assumed in the heat exchanger models (heat losses in the heat exchangers are neglected because of the good thermal insulation). As shown with this example, most of the measured variables are interdependent to each other and there are redundancy constraints which must be verified for every steady-state point. Among others, these constraints include to verify both mass and energy balances in each component, to verify the equality between sensors measuring a same quantity and to ensure feasible temperature profiles in the heat exchangers (i.e. ensure a pinch greater than zero). A reconciliation method is thus applied to define an experimental database that can be used as reference for the calibration of predictive models [28]. The goal of the reconciliation is to correct the measured values as little as possible, while accounting for the sensors accuracy, in order to satisfy the system constraints. Mathematically, it can be formulated as the

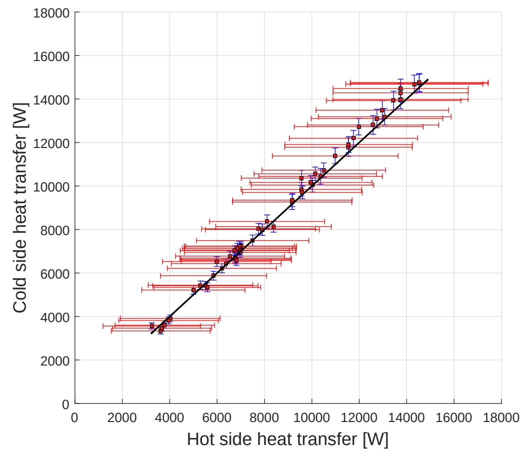

Figure 3: Heat balance of an evaporator evaluated on both hot and cold sides - the blue and red brackets represent the confidence interval when accounting for the sensors accuracy (NB: the wider red intervals of the hot side heat transfer are the result of poorer sensor accuracies)

definition of corrected values c_i which minimize a penalty $f(c_i)$ function i.e.

$$
\begin{aligned}
\min_{c_i} \quad & f(c_i) = \sum_{i=1}^{N} \frac{(m_i - c_i)^2}{\sigma_i^2} \\
\text{s.t.} \quad & \text{. energy balance verified in each component;} \\
& \text{. mass balance verified in each component;} \\
& \text{. measurements redundancy respected;} \\
& \text{. pinch in heat exchangers} > 0;
\end{aligned}
\tag{1}
$$

where m_i are the original measurements, c_i are the corrected values and σ_i are the sensor absolute accuracies. This optimization is performed for every steady-state point of both test rigs. In order to ensure the viability of the reconciliation results, the difference between the corrected values and the original measurements is checked to be within the sensors accuracies. Steady-state points which do not respect this condition, or those whom the optimization failed to respect the constraints in Equation 1, are also eliminated.

Table 3: Operating ranges of the experimental measurements

		Facility ORC_1			Facility ORC_2		
$\dot{m}_{wf}$	$[g/s]$	[15.2	...	68.4]	[277	...	619]
P_{ev}	$[bar]$	[6.47	...	14.3]	[9.8	...	20.5]
P_{cd}	$[bar]$	[1.59	...	6.63]	[2.67	...	4.25]
$T_{htf,h,su}$	$[°C]$	[88	...	119]	[137	...	169]
$T_{htf,c,su}$	$[°C]$	[17.6	...	25.7]	[19.6	...	34.6]
$\dot{W}_{net}$	$[W]$	[16	...	1255]	[875	...	6000]
$\varepsilon_{net,ORC}$	[%]	[0.31	...	8.5]	[1.48	...	4.91]

As a result of this post-treatment process, two experimental datasets of 45 and 44 performance points are obtained for the systems ORC_1 and ORC_2, respectively. These datasets are used as reference to characterize the performance of both facilities in off-design conditions. Ranges of the experimental data are summarized in Table 3 and detailed values of the reconciliated measurements are provided in the appendix (see Appendix A).

3. Modelling methods

The performance of the power ORC systems and their components varies with the operating conditions. In this work, three modelling methods are investigated to simulate each heat exchanger and mechanical device constituting the ORC systems, namely a constant-efficiency method (*CstEff*), a polynomial regression method (*PolEff*) and a semi-empirical method (*SemiEmp*). This list of modelling approach is not exhaustive and many other types of models can be found in the literature. For instance, more complex simulation tools like CFD or advanced deterministic models (i.e. models which account for all the physical and chemical phenomena in the processes) exist to simulate the different components (e.g. [29, 30]). However, these models are often computationally intensive and can hardly be coupled for performing system-level simulations. Since the ultimate goal of this work is the characterisation of complete ORC power plants in off-design conditions, only common modelling approaches that

Table 4: Models inputs, outputs and parameters

Component	Inputs	Outputs	CstEff parameters	PolEff parameters	SemiEmp parameters
Pump	N_{pp}, T_{su}, P_{su}, P_{ex}	$\dot{m}$, $\dot{W}_{mec}$, T_{ex}	$\bar{\varepsilon}_{is,pp}$, $\bar{\varepsilon}_{vol,pp}$, AU_{loss}	AU_{loss}, a_{ij}, b_{ij} with i and $j \in \{1,2\}$	A_{lk}, $\dot{W}_{loss}$, K_{loss}, AU_{loss}
Expander	N_{exp}, T_{su}, P_{su}, P_{ex}	$\dot{m}$, $\dot{W}_{mec}$, T_{ex}	$\bar{\varepsilon}_{is,exp}$, $\bar{\varepsilon}_{vol,exp}$, AU_{loss}	AU_{loss}, c_{ijk}, d_{ijk} with i, j and $k \in \{1,2\}$	d_{su}, AU_{su}, AU_{ex}, AU_{amb} C_{loss}, A_{lk}, $\dot{W}_{loss}$
Heat exchanger	$\dot{m}_h$, $P_{h,su}$, $T_{h,su}$, $\dot{m}_c$, $P_{c,su}$, $T_{c,su}$	$\dot{Q}_{th}$	$\bar{\varepsilon}_{th}$	e_{ij} with i and $j \in \{1,2\}$	$\alpha_{conv,ij}$ and n_{ij} with $i \in \{liq, tp, vap\}$ and $j \in \{h, c\}$

are convenient for system-level simulations are investigated. The assumptions used to perform the modelling are given as below:

- all the components are in steady-state conditions;
- heat losses in the heat exchangers are neglected (good thermal insulation);
- pressure drops in the pipelines and the heat exchangers are lumped at a single place in both the high and low pressure lines;
- heat losses in the pipelines are lumped at a single place in both the high and low pressure lines;
- heat exchangers feature counter-flow patterns;
- a global electromechanical efficiency of the pumps and the expanders of 87% is set in all conditions;
- kinetic and gravitational terms are neglected in the energy balance;

The models are implemented so as to predict the performance of existing devices based on the component supply conditions only. Table 4 summarizes the inputs, independent outputs and parameters of each model. For the sake of conciseness, the constitutive equations of the models are not provided in the text but are available in Appendix B. The following section describes the different models investigated in this work.

3.1. Constant-efficiency models

The first type of models considered in this work assumes constant performance parameters whatever the operating conditions. In the case of the pump and the expander, both the isentropic efficiency ε_{is} and the volumetric efficiency ε_{vol} are imposed as constant values. In order to account for the heat losses in these mechanical components, a third parameter AU_{loss} (representing a global heat transfer coefficient with the ambiance) is added to the models and is kept constant. Regarding the heat exchangers, the maximum heat power transferable between two media is the one leading to a pinch equal to zero. In practice, the effective heat transfer in a heat exchanger is always a fraction (referred to as the thermal efficiency ε_{th}) of this maximum heat power. In order to characterize the different heat exchangers, a constant value is assigned to their respective thermal efficiencies.

3.2. Polynomial-regression models

This second type of models does not impose constant values to the performance parameters (i.e. ε_{is}, ε_{vol}, ε_{th}) but uses instead polynomial regressions to account for the effect of the operating conditions. A second-order multivariate polynomial is applied for every component to keep the methodology systematic. Quadratic functions (i.e. polynomials of degree two) are chosen to limit Runge's phenomenon and over fitting effects. The generic form of the polynomials is

$$\varepsilon = \sum_{i=0}^{2}\sum_{j=0}^{2}\sum_{k=0}^{2} a_{ijk} X^i Y^j Z^k \tag{2}$$

where X, Y and Z are the most representative independent input variables that influence the component efficiency. These variables are identified for each class of component (i.e. the pump, the expander and the heat exchangers) as detailed in the Appendix (Eq. B.8 to B.14).

3.3. Semi-empirical models

Another way for characterizing the ORC components is to use semi-empirical models which implement physics-based equations. While the two previous types of model are empirical, i.e. they implement equations that do not represent the physics of the processes, the semi-empirical models presented here below rely on a limited number of physically meaningful equations whose parameters can be tuned to fit a reference dataset. For instance, the volumetric expanders are simulated by means of the grey-box model proposed by Lemort et al. [31]. Besides of under- and over-expansion losses due to the fixed built-in volumetric ratio of the machine, the model accounts for internal leakages, mechanical losses, pressure drops and heat losses. The pumps are simulated in a similar manner. The effective mass flow delivered by the pump is calculated as an ideal mass flow rate to which an internal recirculation leakage is deduced (Eq. B.15). The mass flow rate characterizing these leakages is modelled by means of an incompressible flow through an equivalent orifice. Finally, the mechanical consumption of the pump is obtained by summing the mechanical losses to the isentropic power (Eq. B.16). Regarding to the heat exchangers, a three-zone moving boundary model with variable heat transfer coefficients is used. The modelling is decomposed into the different zones of the heat exchanger. Each zone is characterized by a global heat transfer coefficient U_i and a heat transfer surface area A_i. The effective heat transfer occurring in the heat exchanger is calculated such as the total surface area occupied by the different zones corresponds to the geometrical surface area of the component (Eq. B.20). In the case of a fin coil heat exchanger (e.g. the condenser of the test-rig ORC_1), the model also accounts for the fin efficiency by implementing Schmidt's theory [32]. Finally, a flow-dependent relationship is used to account for the effect of the fluids mass flow rates on the convective heat transfer coefficients (Eq. B.21).

3.4. Pipeline losses

Besides of the active components constituting the closed-loop cycles (heat exchangers, pumps and expanders), it is also important to account for the losses induced by the interconnecting pipelines in the systems. When modelling the complete ORC facilities (cfr. section 5), these losses are lumped in each line (i.e. high pressure and low pressure) by means of a single artificial component placed at the inlet of the pump and the expander respectively. Pressure losses are simulated as a linear function of the fluid kinetic energy (Eq. B.22) while ambient heat losses are modelled with a single AU_{loss} coefficient as in Eq. B.24.

4. Component-level analysis

The models described here above have varying capabilities to simulate the performance of a same component. In this section, a comparison of the fitting and the extrapolation ability of the different models is applied at the component level, i.e. each component is studied independently to the others. The post-processed experimental measurements described in section 2 are used as reference for both the calibration (i.e. as *training* set) and the evaluation (i.e. as *test* set) of the models.

4.1. Fitting performance

In a first step, the fitting performance of the models (i.e. the ability of the models to fit an experimental database after calibration) is considered. To this end, each component of the two ORC units is simulated by means of the three different models (constant-efficiency, polynomial and semi-empirical) which are each calibrated using *every* experimental point of the reference datasets. The calibration is performed by tuning the model parameters so as to minimize the mean relative errors committed on the different model outputs over the entire calibration domain. The minimization is performed with a derivative-free direct search optimization algorithm. Once calibrated, the residuals between the simulation results (i.e. the models outputs) and the experimental values are analysed. For example, the case of an expander is depicted in Figure 4. The experimental points used for the calibration and the evaluation of the models are illustrated on the left side while the model outputs (i.e. the expander mechanical power, the fluid mass flow rate and the fluid exhaust temperature) are compared to the reference data by means of parity plots. In order to compare numerically the performance of the three types of model, the Root Mean Square Error

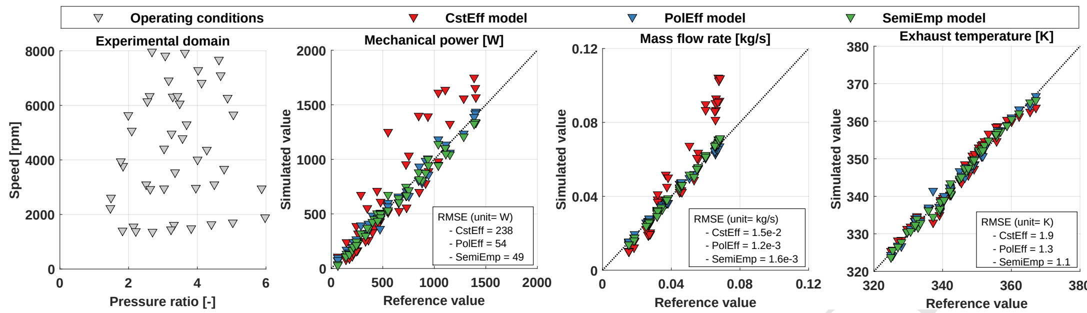

Figure 4: Fitting performance of the expander models. (a) Operating domain of the experimental points (b) parity plot of the mechanical power (c) parity plot of the mass flow rate (d) parity plot of the exhaust temperature

($RMSE$) is evaluated for each model output y, i.e.

$$RMSE_y = \sqrt{\sum_{i=1}^{N} \frac{(\widehat{y}_i - y_i)^2}{N}} \tag{3}$$

where $\widehat{y}_i$ and y_i correspond respectively to the reference and the predicted output values of the i^{th} point for a given model. Although widely used in the literature, the RMSE is a scale-dependent quantity which can only be used to compare the performance of different models for the prediction of a single variable. Furthermore, the RMSE is not a normalized factor and it does not illustrate comprehensively the precision of the models individually. Therefore, the Mean Absolute Percent Error (as defined in Equation 4) is also proposed as figure of merit to characterize the different models.

$$MAPE_y = \frac{1}{N} \sum_{i=1}^{N} \frac{|\widehat{y}_i - y_i|}{\widehat{y}_i} \tag{4}$$

This study, illustrated in the case of an expander, is applied for every component of the two test-rigs and the global results (in terms of RMSE) are given in Figure 5. For the reader's convenience, detailed values of the root mean square errors and the mean absolute percent errors are provided in the Appendix C.

Based on the results, it can be seen that the models have varying success in matching the experimental measurements. In most cases, the constant-efficiency

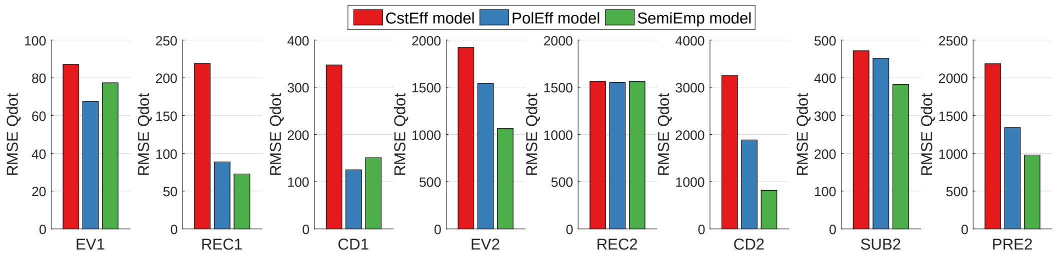

(a) RMSE of the models outputs for the heat exchangers

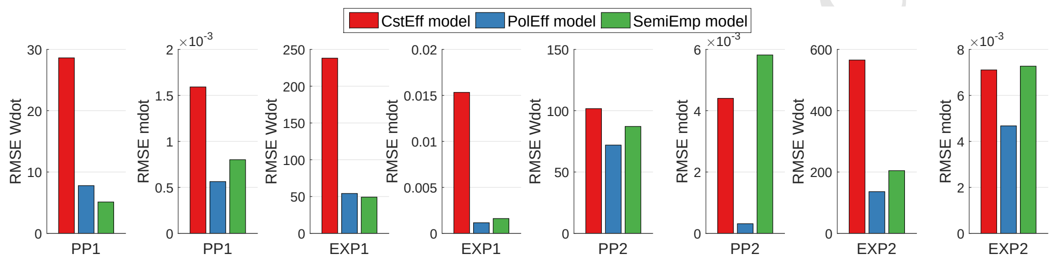

(b) RMSE of the models outputs for the mechanical devices

Figure 5: Fitting performance for the component-level analysis

models lead to the highest simulation residuals. Although straightforward and easy to use, the assumption of invariable components efficiencies should be avoided for off-design modelling. The polynomial and semi-empirical models fit the datasets better but a clear trend cannot be observed. In some cases (e.g. $EV1$ and $CD1$) the polynomial regressions fit the best the dataset, while with other components (e.g. $EV2$ and $PRE2$) the semi-empirical model show the lowest residuals. On average, the absolute percent errors committed while fitting the heat transfer rate in the heat exchangers are 5.9%, 3.5% and 4.1% for the constant-efficiency, the polynomial-based and the semi-empirical models, respectively. Regarding the mechanical devices, these global percent errors are respectively equal to 7.6%, 1.1% and 2.1% for the prediction of the mass flow rate and 21.9%, 7.2% and 7.1% for the mechanical power.

4.2. Extrapolation performance

Additionally to the fitting performance, another key property of the models to be assessed is their capability to predict the components performance in unseen operating conditions. To this end, it is proposed to perform a cross-validation in which the test set is defined outside of the domain of the training set. The experimental points are therefore divided for each component into two subgroups of equal size: an internal training dataset (used to calibrate the models) and an extrapolation testing dataset (used to cross-validate the models outside of the calibration domain). In order to automatically define these internal training and external testing datasets, the following method is applied systematically for each component individually (an illustrative example is given in Figure 6 for the case of a heat exchanger):

1. The experimental points are reported as a point cloud in a 2D graph according to two key variables which illustrate the best the operating conditions of the component. In the case of the heat exchangers, the two variables are the heat power and the pinch point (see Figure 6a), whereas the machine rotational speed and the pressure ratio are used for the mechanical devices.

2. The operating conditions forming the convex envelope of the point cloud are identified and defined as part of the external testing dataset (see Figure 6b). The remaining internal points are kept as potential insiders for further division.

3. Iteratively, this process is repeated to the remaining points until the number of points included in the external testing dataset is equal to half of the points in the dataset (see Figure 6 c-d). Ultimately, the point cloud is divided in two groups of equal size: half of the points in the innermost area of the point cloud form the calibration dataset (blue triangles in Figure 6e), while half of the points in the outermost regions are used

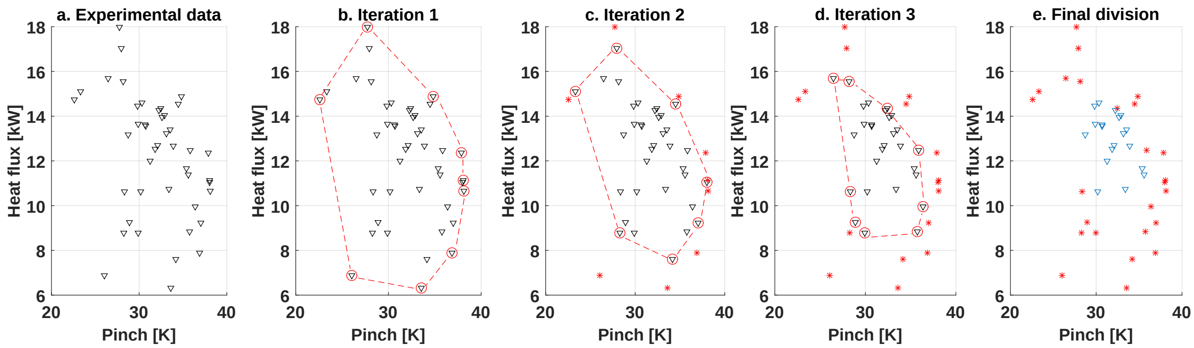

Figure 6: Training and testing data set identification in the case of the recuperator of ORC_2. a) Point cloud of the experimental data. b) First convex envelope calculation; c) Second convex envelope calculation; d) Third convex envelope calculation; e) Final training and testing dataset (with 22 points in each group)

as extrapolation testing dataset (red stars in Figure 6e).

Once these domains are identified, the models are calibrated with data of the training set (using the same methodology as in section 4.1) and then are simulated in the testing set. The example of an expander is depicted in Figure 7 where cross and circle markers refer to the training set and the testing set, respectively. In order to quantify the extrapolation performance of each model, the RMSE and the MAPE are calculated in reference to the extrapolation test set *only*. The same study is applied for every component of both test rigs. The results are given in Figure 8 and detailed values of the RMSE and the mean absolute percent errors are provided in Appendix C.

As in the fitting performance analysis, the constant-efficiency models still demonstrate poor performance. Also, it can be seen that polynomial models do not necessarily lead to the lowest residuals anymore, which highlights a key drawback of these models: the shape of the polynomial laws cannot be controlled out of their calibration domain. On the other hand, semi-empirical models (which implement physically meaningful equations) are much more robust in extrapolation. On average, the percent errors while extrapolating the heat power in the heat exchangers are 7.5%, 5.2% and 5.1% for the constant-efficiency,

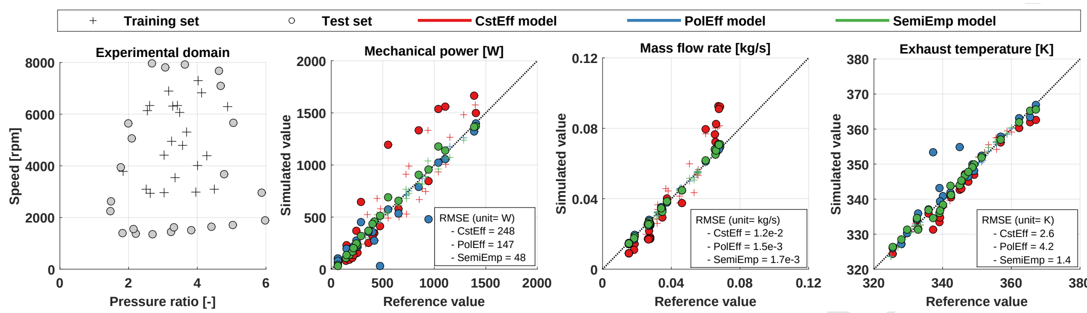

Figure 7: Extrapolation performance of the expander models in the case of ORC_1 (a) Experimental data divided in inner calibration points and outer evaluation points (b) Parity plot of the mechanical power (c) Parity plot of the mass flow rate (d) Parity plot of the exhaust temperature.

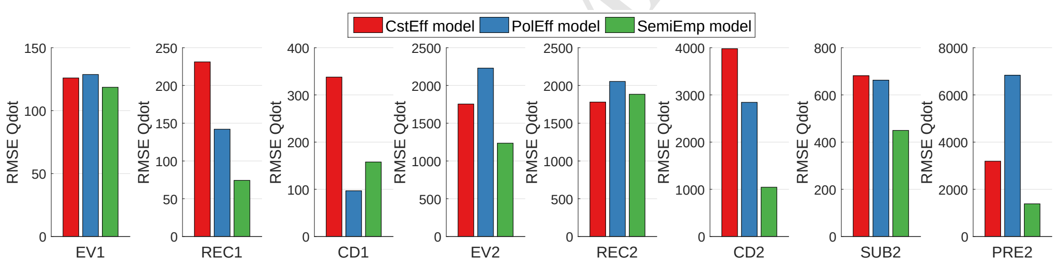

(a) RMSE of the models outputs for the heat exchangers

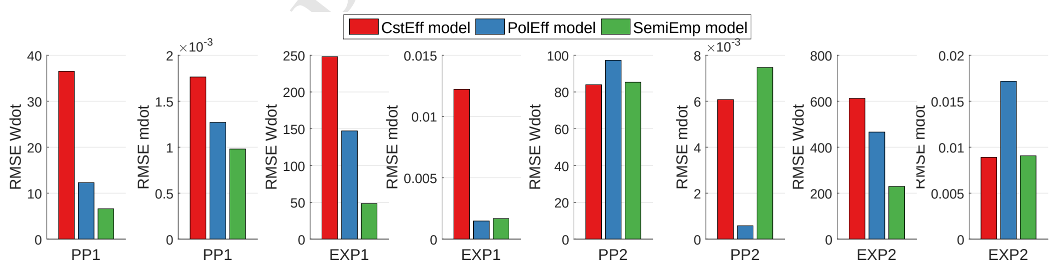

(b) RMSE of the models outputs for the mechanical devices

Figure 8: Extrapolation performance for the component-level analysis - Global results

the polynomials and the semi-empirical models, respectively. Regarding the mechanical devices, the global percent errors committed on the mechanical powers are equal to 29.1%, 14.6% and 8.4% for each model respectively while smaller residuals are observed for the mass flow rates with values of 9.6%, 2.6% and 2.5%.

5. Cycle-level analysis

In practice, models of individual components are often interconnected to simulate larger power systems. In this section, the two ORC units are simulated by coupling in series the models of each sub-component. For each ORC system (ORC_1 and ORC_2), three different models are built (i.e. constant-efficiency, polynomial and semi-empirical) by using the corresponding component models. In order to best replicate the physics of the system, these off-design models are developed in such a way that the complete thermodynamic state of the ORC can be deduced from the boundary conditions only, i.e. the heat source and the heat sink supply conditions, as well as the pump and the expander speeds. The usefulness of such ORC models is very high: they can be used to evaluate the ORC performance over extended range of conditions and, ultimately, to derive the optimal speeds to be set to the different components (pump, expander and condenser fan) in order to maximize the systems power output or net thermal efficiency. Inputs, outputs and parameters of the ORC models are illustrated in Figure 9. The exact mass of refrigerant in the systems being unknown, the ORC models are not made charge sensitive and the subcooling at the condenser outlet is imposed for the different simulations [33]. Apart of the cycle subcooling, there is not any user-defined *intrinsic* assumption of the ORC state (e.g. imposed superheating, refrigerant mass flow rate, condensing or evaporating pressure, etc.). Since the off-design modelling of an ORC is an implicit problem that cannot be formulated causally (because of the multiple interactions between the different components), the thermodynamic states along the cycle are found through an iterative optimization process driving internal key residuals to zero. More specifically, the ORC model iterates on the condensing pressure, the evaporating pressure and the evaporator outlet enthalpy in order to drive the following residuals to a value lower than 10^{-6}:

$$res_1 = 1 - \frac{\dot{m}_{pp,sim}}{\dot{m}_{exp,sim}} \tag{5}$$

$$res_3 = 1 - \frac{h_{cd,ex}}{h_{cd,ex,2}} \tag{6}$$

$$res_3 = 1 - \frac{h_{ev,ex}}{h_{ev,ex,2}} \tag{7}$$

The solver architecture is depicted in Figure 9 and further information about the ORC model can be found in the ORCmKit documentation [22]. As in the component-level analysis, both the fitting and the extrapolation performance of the three modelling approaches are evaluated while simulating the entire power systems.

5.1. Fitting performance

The ability of the three ORC models to fit the experimental datasets is first investigated. To this end, the models of the different components calibrated with the complete database (i.e. the ones presented in section 4.1) are coupled together to form the three ORC models. These ORC models are then evaluated in the same operating conditions than the experimental points while only accounting for the external boundary variables. The system performance predicted by each modelling approach are finally compared with the experimental data. For example, experimental and predicted T-s diagrams are shown in Figure 10 for two different operating conditions. In the first case (left), it can be seen that the three models replicate well the experimental conditions in terms of temperature and pressure. The second example (right), on the other hand, demonstrates larger discrepancies between the simulation results despite of the identical operating conditions.

In order to numerically quantify the performance of the different models, RMSEs and MAPEs are calculated for the various energy flows involved in the

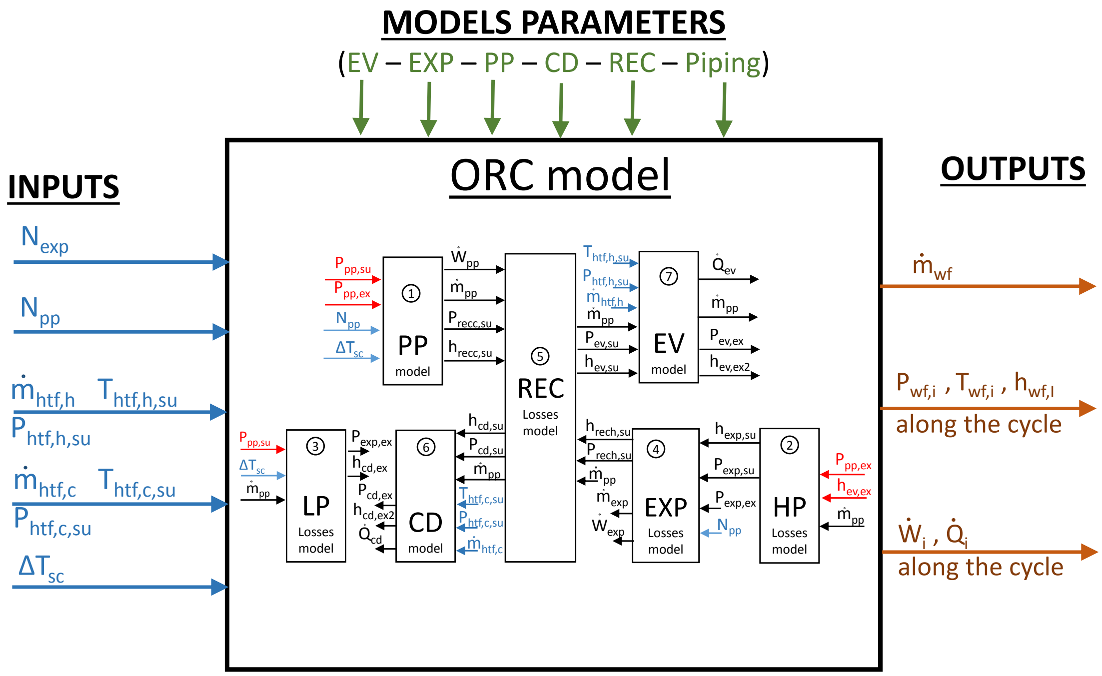

Figure 9: Inputs (in blue), outputs (in brown), parameters (in green), iteration variables (in red) and solver architecture of the cycle model (case of the facility ORC_1). The circled number in each component model informs the execution order of the model .

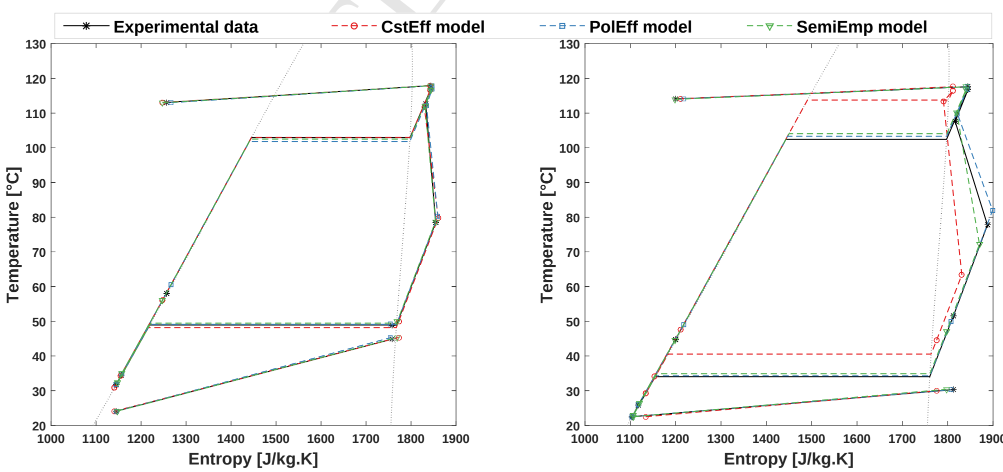

Figure 10: T-s diagrams predicted by the three ORC models for the system ORC_1 (left) experimental point #32 (right) experimental point #36

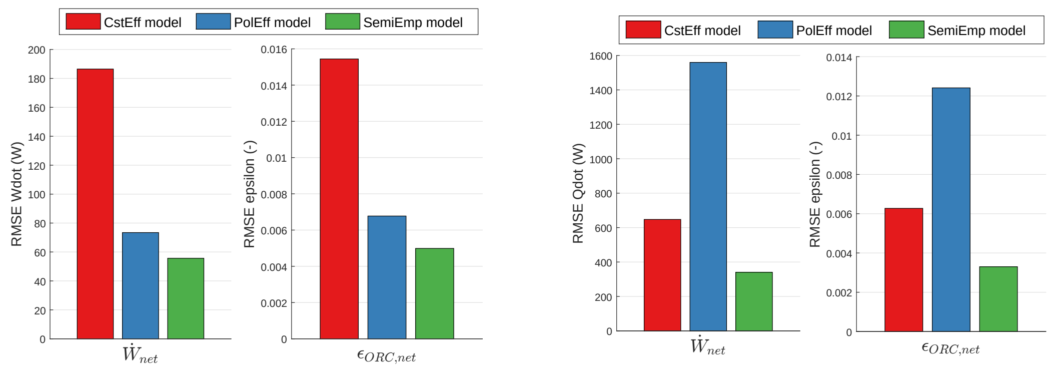

(a) RMSE of the models outputs - ORC 1

(b) RMSE of the models outputs - ORC 2

Figure 11: Fitting performance for the cycle-level analysis - Global results

two systems and detailed values of these performance indicators are provided in Appendix C. In comparison to the results presented in section 4.1, it is observed that the residuals when modelling the complete ORC power systems are larger than in the component-level analysis (the RMSEs are 2.3 times higher on average). Such increase is due to the propagation and addition of the sub-model errors along the ORC. Unlike the component-level analysis which compared each component individually with identical supply conditions, here the models inputs and outputs are interdependent.

When considering a complete ORC system, two common variables used to evaluate the global machine performance are the net mechanical power $\dot{W}_{net}$ generated by the engine and the net cycle efficiency ε_{ORC}, i.e.

$$\varepsilon_{ORC} = \frac{\dot{W}_{net}}{\dot{Q}_{in}} \tag{8}$$

where $\dot{Q}_{in}$ is the total heat power supplied to the system. RMSEs committed by the three ORC models to replicate these performance outputs are depicted in Figure 11. In the case of the first ORC system (ORC_1), similar conclusions to the component-level analysis can be drawn. The constant-efficiency ORC model leads to the highest simulation residuals while the polynomial-based and

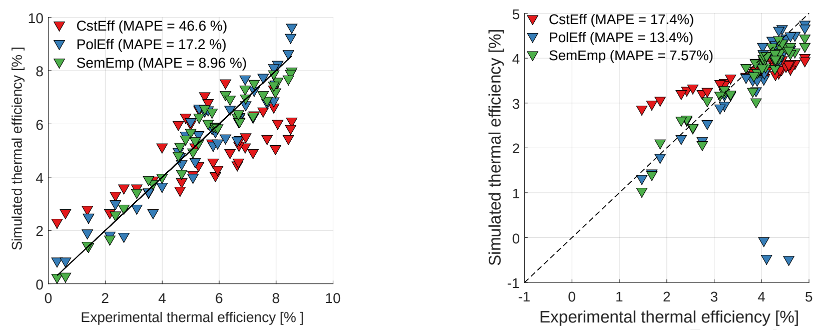

(a) Thermal efficiency of system ORC 1

(b) Thermal efficiency of system ORC 2

Figure 12: Parity plots of the thermal efficiency predicted by the three types of model for both ORC units.

the semi-empirical models offer better simulation performance. On the other hand, results related to the second system (ORC_2) are different and highlight a major drawback of the polynomial-based ORC model. In some cases, the cycle state into which the residuals (as given in Eqs. 5 - 7) are driven to zero may be out of the calibration domain of some the subcomponents model. However, as it as been mentioned previously, polynomial regressions do not ensure any reliable results in extrapolation. Therefore, the polynomial-based ORC model may commit significant deviations compared to the reference data, even though it is re-evaluated in the same operating conditions used for to calibrate the subcomponents models. The robustness of an ORC model built by the interconnection of multiple polynomial regressions cannot be ensured in all cases. Regarding the semi-empirical ORC model, much better robustness is observed and good fitting performance are demonstrated with both ORC facilities.

Finally, the net efficiency predicted by the three modelling approaches for the two test rigs are compared to the experimental data in Figure 12. Although the ORC system models are re-evaluated on the calibration conditions (i.e. the reference conditions used to calibrate each subcomponent models), significant residuals can be observed. More specifically, the average percent error committed on the net thermal efficiency by the constant-efficiency, the polynomial-based and the semi-empirical ORC models are 32%, 15.3% and 8.3%, respectively. Such high values result from the accumulation of errors which affect the different variables involved in the calculation of the net efficiency. In conclusion, even though the models of the different components are well calibrated independently, the net thermal efficiency predicted by the cycle model can present significant deviations, the highest average error being stated for the constant-efficiency ORC model.

5.2. Extrapolation performance

Finally, the capability of the three ORC models to extrapolate the whole system performance in unseen operating conditions is analysed. The cross-validation methodology used to perform this study is identical to the component-level analysis discussed in section 4.2. For each ORC facility, the experimental data are divided in two subgroups of equal size: an internal training dataset (used to calibrate the different component models) and an extrapolation testing dataset (used to cross-validate the ORC models outside of the calibration domain). However, it must be noted that the models calibrated in the extrapolation analysis at the component-level cannot be coupled together to perform the same analysis at the cycle-level. Indeed, the training sets defined for each component (as presented in section 4.2) and used to calibrate the various models are not identical. For instance, while considering the system ORC_1, the experimental point #4 is defined in the training set of the pump, but it is considered as external from the evaporator point of view. In order to make the study consistent, a common training set must be defined for all the components of a same ORC engine. To this end, the experimental points are first reported in a 2D graph accordingly to the net power output and the cycle thermal efficiency, then the method based on an iterative evaluation of the convex envelope is applied until groups of equal size are obtained (cfr. section 4.2 for further explanations). As an example, the final data division performed for the first ORC facility (ORC_1) is depicted in Figure 13. The different component models are

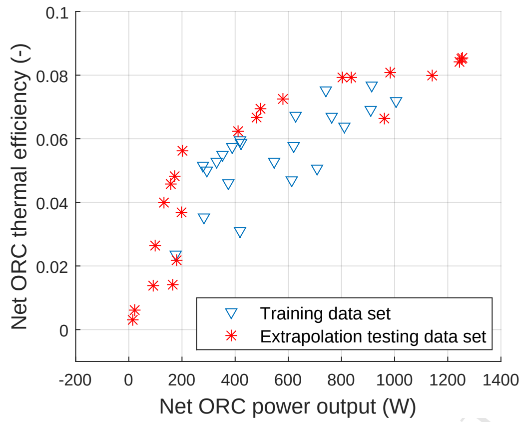

Figure 13: Data division of the system ORC_1 for the extrapolation analysis

then calibrated using data of the internal training set and the component models are coupled together to form the complete ORC power unit. The three types of ORC models are finally simulated in the operating conditions of the test set (i.e. in extrapolation) only. Similarly as before, RMSEs and MAPEs committed on the different energy flows in the two systems are provided in Appendix C. Like in the fitting performance analysis (see section 5.1), the residuals committed on the net power output and the net cycle efficiency are investigated and the related RMSEs committed by each modelling method are depicted in Figure 14. It can be seen that, for both facilities, the constant-efficiency ORC model leads to the highest residuals while the semi-empirical ORC model demonstrates the best extrapolation capability. The polynomial-based ORC model presents intermediate performance but, as it has been highlighted previously, viable results cannot be ensured out of the calibration range (although convergence issues are not observed with the current simulations). Quantitatively speaking, the average percent errors committed on the net thermal efficiency by the constant-efficiency, the polynomial-based and the semi-empirical ORC models are 51.2%, 19% and 14.2%, respectively.

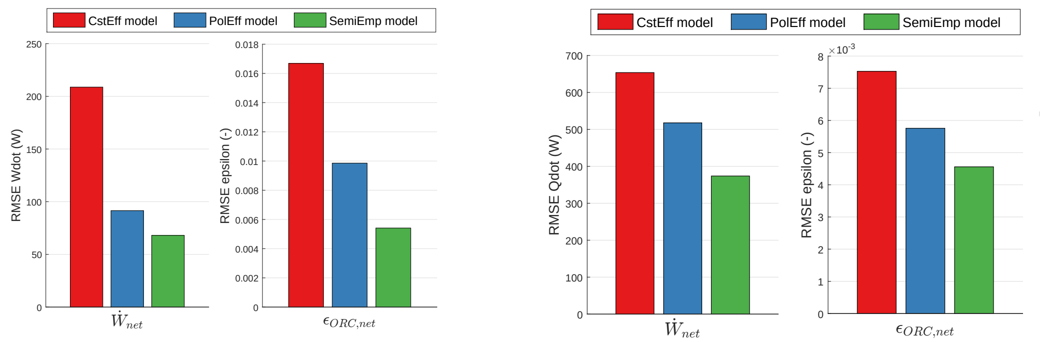

(a) RMSE of the models outputs - ORC 1

(b) RMSE of the models outputs - ORC 2

Figure 14: Extrapolation performance for the cycle-level analysis - Global performance results

6. Computational efficiency

This last section is dedicated to the computational performance of the different modelling methods. The model computational time can indeed be a crucial parameter if the model is used e.g. for Monte Carlo simulations, in control optimization problems, or integrated into a larger system model. As a figure of comparison, average computational times of the different models presented through the text are summarized in Table 5. These values should be considered as a qualitative indicator only, since they depend on the equations implementation and the computer performance. It can be seen that the higher the model complexity, the higher the simulation time. Constant-efficiency and polynomial-based models show very similar computational efforts because of the fast calculation of the polynomial regressions. On the other hand, semi-empirical model (which often require implicit iterations and additional call to the working fluid thermodynamic properties) are characterized by longer running times (4 times higher for the heat exchanger model and more than 100 times higher for the expander model). Regarding the ORC system models, similar trends are observed at a greater magnitude. Besides of implicitly solving the components models, the ORC models also require internal iterations in order to derive the system steady-state performance based on the boundary conditions only.

Table 5: Mean simulation times of the different modelling methods to evaluate one operating point (simulations performed with a laptop Dell Latitude E5450, CPU Intel Core i7-5600U 2.6GHz, 8GB RAM)

	Pump	Expander	Heat Exchanger	ORC
CstEff model	9.5×10^{-4} sec	9.1×10^{-4} sec	9.9×10^{-3} sec	1.1×10^{1} sec
PolEff model	1.1×10^{-3} sec	1.1×10^{-3} sec	1.2×10^{-2} sec	1.4×10^{1} sec
SemiEmp model	1.2×10^{-3} sec	1.1×10^{-1} sec	4.1×10^{-2} sec	3.5×10^{1} sec

7. Conclusions

Among the many topics of research and development in the energy sector, power generation from low-grade heat sources is gaining interest and the organic Rankine cycle (ORC) is seen as one of the most suitable technology for such applications. Aside of proper fluid selection and system design, the off-design characterization and control of ORC power systems is important due to the versatile nature of their operating conditions. Because of the incompleteness of the experimental data, mathematical modelling tools are often required to predict the system performance as a function of the boundary working conditions. To this end, a wide range of modelling paradigms can be chosen to simulate the power plants and their sub-components. In this work, it is proposed to analyse and compare three modelling methods to simulate in off-design conditions ORC-based power plants and their constitutive components (heat exchangers, pumps and expanders), namely

- a *constant-efficiency method* which assumes constant components efficiencies whatever the operating conditions;
- a *polynomial regressions method* which adapt the components efficiencies to the operating conditions by means of quadratic functions (second-order multivariate polynomials);
- a *semi-empirical method* which simulate the components by means of a limited number of physically-meaningful equations.

These models are compared in terms of fitting and extrapolation performance. To this end, experimental measurements gathered on two ORC facilities are post-processed and used as reference for the models calibration and evaluation. Both root mean square errors (RMSEs) and mean absolute percent errors (MAPEs) are calculated for the sake of model comparison. The analysis is first performed at a component level (i.e. each pump, heat exchanger and expander is studied individually) and then extended to the entire ORC power units. Numerical results drawn from the study can be summarized as follows:

1. In the component-level analysis, the absolute percent errors committed while *fitting* the heat transfer in the heat exchangers are on average 5.9%, 3.5% and 4.1% for the constant-efficiency, the polynomial and semi-empirical models, respectively. Regarding the mechanical devices, these global percent errors are respectively equal to 7.6%, 1.1% and 2.1% for the prediction of the mass flow rate and 21.9%, 7.2% and 7.6% for the mechanical power.

2. In the component-level analysis again, it is demonstrated that the modelling residuals are increased when using the models outside of the calibration domain (i.e. in extrapolation). More specifically, the percent errors while *extrapolating* the thermal power in the heat exchangers are on average 7.5%, 5.2% and 5.1% for the constant-efficiency, the polynomials and the semi-empirical models respectively. Regarding the mechanical devices, the average percent errors committed on the mechanical powers are equal to 29.1%, 14.6% and 8.4% for each model respectively while smaller residuals are observed for the mass flow rates with values of 9.6%, 2.6% and 2.5%.

3. Because of the propagation of the models uncertainties, RMSEs of the residuals are on average 2.3 higher when modelling the complete systems in comparison to the results of the component-level analysis.

4. When modelling the entire ORC power systems in the reference boundary conditions, the average percent error committed on the net thermal efficiency is equal to 32%, 15.3% and 8.3% for the constant-performance, the polynomial and the semi-empirical ORC models respectively. Such high values result from the accumulation of errors which affect the different variables involved in the calculation of the net efficiency.

5. Like in the component-level analysis, it is seen that the simulation residuals are increased while using the ORC models in extrapolation. The average percent errors committed on the net thermal efficiency rise to 51.2%, 19% and 14.2% for the constant-performance, the polynomial and the semi-empirical ORC models respectively.

Although they are fast to implement, to calibrate and to compute, it can be seen that constant-efficiency models demonstrate poor performance for both component- and cycle-level simulations. In most cases, they lead to the highest residuals and should only be considered for off-design simulation if the operating conditions remain close to the nominal operating point. Polynomial-based models are also fast to calibrate and to evaluate. They reveal very good fitting performance while considering the components individually. However, polynomial-based models can be unreliable in extrapolation and when coupled together. They should only be used for characterizing the components individually and within their calibration ranges for interpolation modelling. Semi-empirical models, on the other hand, show good and robust performance in both fitting and extrapolation at both component- and cycle-level analysis.

Based on the current study, semi-empirical models demonstrate to be the most suitable for the off-design simulation of ORC systems despite of the higher calibration and simulation times. The proper simulation for a particular application results from the classic trade-off between accuracy and complexity. The selected model should be accurate enough for the purpose of the simulation, but its limitations should be known from the modeller. It is important to note that the modelling approaches investigated in this work are not exhaustive. Other forms of correlations can be used to characterize the components efficiencies (e.g. first- or third-order multivariate polynomials, more complex regressions of the expander efficiency [34], etc.) and models of different class could be coupled together to simulate the closed-loop systems.

Finally, it must be noted that the system-level simulations are performed by imposing the cycles sub-cooling in the ORC model. Since the goal of this work is only to compare different modelling paradigms, such a simplification is considered acceptable as it does not biased the analysis. However, in order to perform valuable off-design simulations, the ORC model should be improved to be charge sensitive, i.e. it imposes the total mass of refrigerant enclosed in the ORC systems instead of the condenser sub-cooling. This particular point highlights another limitation of the simplest modelling approaches presented in this paper: neither the constant-efficiency nor the polynomial-efficiency models permit to properly estimate the amount of refrigerant enclosed in the various heat exchangers. Since these models do not rely on any heat transfer coefficient, they do not calculate the volume fraction occupied by each fluid phase in the heat exchangers, therefore the refrigerant mass enclosed in the heat exchanger cannot be properly computed. Only the semi-empirical model of the heat exchangers (the one based on convective heat transfer coefficients characterizing both fluids) may be used to perform a reliable charge sensitive modelling of the ORC systems. Prospective works include the development and the experimental validation of such a charge-sensitive ORC model.

Acknowledgements

R. Dickes thanks the Fund for Scientific Research of Belgium (F.R.S - F.N.R.S) for its financial support (research fellowship). The authors also would like to gratefully acknowledge the contributors to the Sun2Power project (CMI group, Enertime, Emerson, ACTE and Honeywell) as well as Exoes for sharing the experimental measurements gathered on the Microsol CSP-ORC power plant.

Nomenclature

Acronyms and abbreviations

CD	Condenser
CFD	Computational Fluid Dynamics
CSP	Concentrated Solar Power
CstEff	Constant-Efficiency
EV	Evaporator
EXP	Expander
FS	Full Scale
HEX	Heat Exchanger
HP	High Pressure
HTF	Heat Transfer Fluid
LP	Low Pressure
MAPE	Mean Absolute Percent Error
ORC	Organic Rankine Cycle
PolEff	Polynomial-Efficiency
PP	Pump
PRE	Preheater
REC	Recuperator
RMSE	Root Mean Square Error
SemiEmp	Semi Emperical
SUB	Root Mean Square Error

VFD Variable Frequency Drive

WF Working Fluid

Subcripts and supercripts

amb ambient

c cold

cd condenser

conv convective

dis displacement

ev evaporator

ex exhaust

exp expander

h hot

htf heat transfer fluid

i,j,k index

in incoming

is isentropic

liq liquid

lk leakage

log logarithmic

loss losses

max maximum

mec mechanical

net	net
nom	nominal
pp	pump
rec	recuperator
sc	subcooling
sim	simulated
su	supply
th	thermal
tp	two-phase
vap	vapour
vol	volumetric
wf	working fluid

Variables

α	Heat transfer coefficients, $W/m^2.K$
Δ	Differential, $-$
$\dot{m}$	Mass flow, kg/s
$\dot{Q}$	Heat Power, W
$\dot{V}$	Volume flow rate, m^3/s
$\dot{W}$	Power, W
ρ	Density, kg/m^3
σ	Sensor accuracy, %
ε	Efficiency, %

φ Fluid kinetic energy, $kg.m^3/s^2$

$\widehat{y}$ reference output, $-$

A Surface area, m^2

C Torque, Nm

c Corrected measurements

d Diameter, m

h Enthalpy, J/kg

K, B Model parameters, $-$

m Raw measurements, $-$

N Rotational speed, kg/s

P Pressure, Pa

r_p Pressure ratio, $-$

s Entropy, J/K

T Temperature, K

U Heat transfer coefficient, $W/m^2.K$

V Volume, m^3

X, Y, Z Symbolic variables, $-$

y model output, $-$

a,b,c,d,e Polynomial coefficients, $-$

n Exponent coefficient, $-$

References

[1] B. F. Tchanche, G. Lambrinos, A. Frangoudakis, G. Papadakis, Low-grade heat conversion into power using organic Rankine cycles - A review of various applications, Renewable and Sustainable Energy Reviews 15 (8) (2011) 3963–3979. doi:10.1016/j.rser.2011.07.024.
URL http://www.sciencedirect.com/science/article/pii/S1364032111002644

[2] F. W. Ofeldt, 'Engine' - US Patent No 611792A (1898).
URL http://www.google.ch/patents/US611792

[3] L. Y. Bronicki, Short review of the long history of ORC power systems, in: Keynote lecture of the 2nd International seminar on ORC power systems - ASME-ORC 2013, Rotterdam (NL), 2013.

[4] P. Colonna, E. Casati, C. Trapp, T. Mathijssen, J. Larjola, T. Turunen-Saaresti, A. Uusitalo, Organic Rankine Cycle Power Systems: from the Concept to Current Technology, Applications and an Outlook to the Future, Journal of Engineering for Gas Turbines and Power 137 (October) (2015) 1–19. doi:10.1115/1.4029884.
URL http://gasturbinespower.asmedigitalcollection.asme.org/article.aspx?doi=10.1115/1.4029884

[5] H. Gurgenci, Performance of power plants with organic Rankine cycles under part-load and off-design conditions, Solar & Wind Technology 36 (1) (1986) 45–51. doi:10.1016/0038-092X(86)90059-9.
URL http://www.sciencedirect.com/science/article/pii/0038092X86900599

[6] J. Wang, Z. Yan, P. Zhao, Y. Dai, Off-design performance analysis of a solar-powered organic Rankine cycle, Energy Conversion and Management 80 (2014) 150–157. doi:10.1016/j.enconman.2014.01.032.
URL http://dx.doi.org/10.1016/j.enconman.2014.01.032

[7] F. Calise, C. Capuozzo, A. Carotenuto, L. Vanoli, Thermoeconomic analysis and off-design performance of an organic Rankine cycle powered by medium-temperature heat sources, Solar Energy 103 (2013) 595–609. doi:10.1016/j.solener.2013.09.031.
URL http://dx.doi.org/10.1016/j.solener.2013.09.031

[8] B. R. Fu, S. W. Hsu, Y. R. Lee, J. C. Hsieh, C. M. Chang, C. H. Liu, Performance of a 250 kW organic rankine cycle system for off-design heat source conditions, Energies 7 (6) (2014) 3684–3694. doi:10.3390/en7063684.

[9] D. Hu, Y. Zheng, Y. Wu, S. Li, Y. Dai, Off-design performance comparison of an organic Rankine cycle under different control strategies, Applied Energy 156 (2015) 268–279. doi:10.1016/j.apenergy.2015.07.029.
URL http://www.sciencedirect.com/science/article/pii/S0306261915008582

[10] G. Manente, A. Toffolo, A. Lazzaretto, M. Paci, An Organic Rankine Cycle off-design model for the search of the optimal control strategy, Energy 58 (2013) 97–106. doi:10.1016/j.energy.2012.12.035.
URL http://dx.doi.org/10.1016/j.energy.2012.12.035

[11] J. Sun, W. Li, Operation optimization of an organic rankine cycle (ORC) heat recovery power plant, Applied Thermal Engineering 31 (11-12) (2011) 2032–2041. doi:10.1016/j.applthermaleng.2011.03.012.
URL http://www.sciencedirect.com/science/article/pii/S135943111100144X

[12] S. Quoilin, Sustainable Energy Conversion Through the Use of Organic Rankine Cycles for Waste Heat Recovery and Solar Applications, Ph.D. thesis, University of Liège (2011).

[13] D. Wei, X. Lu, Z. Lu, J. Gu, Dynamic modeling and simulation of an Organic Rankine Cycle (ORC) system for waste heat recovery, Applied Thermal Engineering 28 (10) (2008) 1216–1224. doi:10.1016/j.applthermaleng.2007.07.019.

[14] S. Quoilin, R. Aumann, A. Grill, A. Schuster, V. Lemort, H. Spliethoff, Dynamic modeling and optimal control strategy of waste heat recovery Organic Rankine Cycles, Applied Energy 88 (6) (2011) 2183–2190. doi:10.1016/j.apenergy.2011.01.015.
URL http://dx.doi.org/10.1016/j.apenergy.2011.01.015

[15] J. Zhang, W. Zhang, G. Hou, F. Fang, Dynamic modeling and multivariable control of organic Rankine cycles in waste heat utilizing processes, Computers and Mathematics with Applications 64 (5) (2012) 908–921. doi:10.1016/j.camwa.2012.01.054.
URL http://dx.doi.org/10.1016/j.camwa.2012.01.054

[16] H. Xie, C. Yang, Dynamic behavior of Rankine cycle system for waste heat recovery of heavy duty diesel engines under driving cycle, Applied Energy 112 (2013) 130–141. doi:10.1016/j.apenergy.2013.05.071.
URL http://dx.doi.org/10.1016/j.apenergy.2013.05.071

[17] M. O. Bamgbopa, E. Uzgoren, Numerical analysis of an organic Rankine cycle under steady and variable heat input, Applied Energy 107 (2013) 219–228. doi:10.1016/j.apenergy.2013.02.040.
URL http://dx.doi.org/10.1016/j.apenergy.2013.02.040

[18] N. Mazzi, S. Rech, A. Lazzaretto, Off-design dynamic model of a real Organic Rankine Cycle system fuelled by exhaust gases from industrial processes, Energy 90 (2015) 537–551. doi:10.1016/j.energy.2015.07.083.
URL http://www.sciencedirect.com/science/article/pii/S0360544215009780

[19] A. Hernandez, A. Desideri, C. Ionescu, S. Quoilin, V. Lemort, R. De Keyser, Towards the optimal operation of an organic Rankine cycle unit by means of model predictive control, Proceedings of the 3rd International Seminar on ORC Power Systems (2015) 1–10.

[20] P. Tona, J. Peralez, Control of Organic Rankine Cycle Systems on board Heavy-Duty Vehicles: a Survey, IFAC-PapersOnLine 48 (15) (2015)

419–426. doi:10.1016/j.ifacol.2015.10.060.
URL http://linkinghub.elsevier.com/retrieve/pii/S2405896315019369

[21] T. Erhart, U. Eicker, D. Infield, Part-load characteristics of Organic-Rankine-Cycles, in: 2nd European Conference on Polygeneration, Tarragona (Spain), 2011, pp. 1–11.

[22] R. Dickes, D. Ziviani, M. de Paepe, M. van den Broek, S. Quoilin, V. Lemort, ORCmKit : an open-source library for organic Rankine cycle modelling and analysis, in: Proceedings of ECOS 2016, Portoroz (Solvenia), 2016.

[23] I. H. Bell, J. Wronski, S. Quoilin, V. Lemort, Pure and pseudo-pure fluid thermophysical property evaluation and the open-source thermophysical property library coolprop, Industrial and Engineering Chemistry Research 53 (6) (2014) 2498–2508.

[24] E. Georges, S. Declaye, O. Dumont, S. Quoilin, V. Lemort, Design of a small-scale organic Rankine cycle engine used in a solar power plant, International Journal of Low-Carbon Technologies 8 (2013) 34–41. doi:10.1093/ijlct/ctt030.

[25] R. Dickes, O. Dumont, S. Declaye, S. Quoilin, I. Bell, V. Lemort, Experimental investigation of an ORC system for a micro-solar power plant, in: Proceedings of the 22nd International Compressor Engineering at Purdue, Purdue (USA), 2014.
URL http://hdl.handle.net/2268/170508

[26] V. Rieu, Microsol - A 10 kW solar power plant for rural electrification, in: Presentation at the SolarPACES 2012 conference, Marrakech, 2012.

[27] S. Quoilin, J. Schrouff, Assessing steady-state, multivariate thermo-fluid experimental data using Gaussian Processes: the GPExp open-source library, Energies 9 (6) (2016) –. doi:10.3390/en9060423.

[28] O. Dumont, S. Quoilin, V. Lemort, Importance of the reconciliation method to handle experimental data : application to a reversible heat pump / organic Rankine cycle unit integrated in a positive energy building, International Journal of Energy and Environmental Engineeringdoi: 10.1007/s40095-016-0206-4.
URL "http://dx.doi.org/10.1007/s40095-016-0206-4

[29] M. M. Aslam Bhutta, N. Hayat, M. H. Bashir, A. R. Khan, K. N. Ahmad, S. Khan, CFD applications in various heat exchangers design: A review, Applied Thermal Engineering 32 (1) (2012) 1–12. doi:10.1016/j.applthermaleng.2011.09.001.
URL http://dx.doi.org/10.1016/j.applthermaleng.2011.09.001

[30] R. Dickes, Design and fabrication of a variable wall thickness two-stage scroll expander to be integrated in a micro-solar power plant, Master thesis, University of Liege (2013).
URL http://hdl.handle.net/2268/160458

[31] V. Lemort, S. Quoilin, C. Cuevas, J. Lebrun, Testing and modeling a scroll expander integrated into an Organic Rankine Cycle, Applied Thermal Engineering 29 (14-15) (2009) 3094–3102. doi:10.1016/j.applthermaleng.2009.04.013.
URL http://dx.doi.org/10.1016/j.applthermaleng.2009.04.013

[32] T. Schmidt, Heat Transfer Calculations for Extended Surfaces, ASHRAE Journal (1949) 351–357.

[33] D. Ziviani, B. Woodland, E. Georges, E. Groll, J. Braun, W. Horton, M. van den Broek, M. De Paepe, Development and a Validation of a Charge Sensitive Organic Rankine Cycle (ORC) Simulation Tool, Energies 9 (6) (2016) 389. doi:10.3390/en9060389.
URL http://www.mdpi.com/1996-1073/9/6/389

[34] S. Declaye, S. Quoilin, L. Guillaume, V. Lemort, Experimental study on an open-drive scroll expander integrated into an ORC (Organic Rankine

Cycle) system with R245fa as working fluid, Energy 55 (2013) 173–183. doi:10.1016/j.energy.2013.04.003.
URL http://dx.doi.org/10.1016/j.energy.2013.04.003

Appendix A. Experimental measurements

In this appendix, the reference database obtained experimentally on the test rigs (see section 2) are provided. The reconciliated experimental measurements are summarized in Tables A.6 and A.7 for the first and the second ORC system respectively.

Appendix B. Models constitutive equations

This appendix provides the constitutive equations of the models presented in section 3. Please refer to the nomenclature (see p. 38) for any details regarding the variables names.

Appendix B.1. Constant-efficiency models

– Pump model:

$$\varepsilon_{is,pp} = \frac{\dot{m}_{pp}(h_{ex,is,pp} - h_{su,pp})}{\dot{W}_{mec,pp}} = \bar{\varepsilon}_{is,pp} \tag{B.1}$$

$$\varepsilon_{vol,pp} = \frac{\dot{V}_{su,pp}}{N_{pp} V_{dis,pp}} = \bar{\varepsilon}_{vol,pp} \tag{B.2}$$

$$\dot{W}_{mec,pp} = \dot{m}_{pp}(h_{ex,pp} - h_{su,pp}) + AU_{loss}(\bar{T}_{pp} - T_{amb}) \tag{B.3}$$

– Expander model:

$$\varepsilon_{is,exp} = \frac{\dot{W}_{mec,exp}}{\dot{m}_{exp}(h_{su,exp} - h_{ex,is,exp})} = \bar{\varepsilon}_{is,exp} \tag{B.4}$$

$$\varepsilon_{vol,exp} = \frac{\dot{V}_{su,exp}}{N_{exp} V_{dis,exp}} = \bar{\varepsilon}_{vol,exp} \tag{B.5}$$

$$\dot{m}_{exp}(h_{su,exp} - h_{ex,exp}) = \dot{W}_{mec,exp} + AU_{loss}(\bar{T}_{exp} - T_{amb}) \tag{B.6}$$

– Heat exchanger model:

$$\varepsilon_{th} = \frac{\dot{Q}}{\dot{Q}_{max}} = \bar{\varepsilon}_{th} \tag{B.7}$$

Table A.6: Reconciliated measurements gathered on the test rig ORC_1

$Point\ \#$	N_{exp}	N_{pp}	$\dot{W}_{exp}$	$\dot{W}_{pp}$	$T_{htf,c,ex}$	$T_{htf,c,su}$	$T_{htf,h,ex}$	$T_{htf,h,su}$	$T_{cd,su}$	$T_{exp,ex}$	$T_{exp,su}$	$T_{ev,ex}$	$T_{ev,su}$	$T_{pp,ex}$	$T_{pp,su}$	$P_{exp,ex}$	$P_{exp,su}$	$P_{pp,ex}$	$P_{pp,su}$	$\dot{m}_{htf,c}$	$\dot{m}_{htf,h}$	$\dot{m}_{wf}$
$[-]$	$[rpm]$	$[rpm]$	$[W]$	$[W]$	$[^\circ C]$	$[^\circ C]$	$[^\circ C]$	$[^\circ C]$	$[^\circ C]$	$[^\circ C]$	$[^\circ C]$	$[^\circ C]$	$[^\circ C]$	$[^\circ C]$	$[^\circ C]$	$[bar]$	$[bar]$	$[bar]$	$[bar]$	$[kg/s]$	$[kg/s]$	$[g/s]$
1	3680	240	652	70	22.6	17.6	93.4	97.3	32.9	59.7	91.0	96.6	38.2	19.2	17.9	1.76	8.39	8.67	1.62	1.45	0.96	34.94
2	1890	200	475	63	22.2	18.1	102.9	106.3	39.5	64.0	96.5	105.4	37.2	19.6	18.1	1.67	9.98	10.24	1.59	1.45	0.93	27.82
3	1700	200	420	67	30.0	18.8	102.5	105.7	39.4	66.0	96.5	104.8	41.5	22.5	21.7	2.06	10.37	10.59	2.05	0.51	0.94	27.82
4	1620	200	359	65	43.3	20.2	102.4	105.4	47.4	69.2	96.3	104.6	50.2	31.0	32.7	3.18	10.57	10.74	3.18	0.22	0.92	26.86
5	1554	200	255	56	61.9	21.3	103.6	106.4	63.6	75.5	96.3	105.5	60.2	43.3	48.0	5.12	10.99	11.11	5.12	0.11	0.92	26.30
6	1640	200	399	70	34.3	19.5	101.7	104.8	39.6	66.0	96.0	104.0	44.1	25.1	24.8	2.40	10.60	10.72	2.40	0.37	0.94	27.46
7	7680	400	1041	130	26.6	18.3	99.8	106.4	37.4	67.0	99.1	102.5	46.9	20.4	19.1	2.30	10.66	11.15	1.76	1.44	0.94	59.95
8	7300	400	939	128	33.8	18.8	100.2	106.4	41.7	66.2	96.5	99.7	49.8	23.8	22.9	2.65	10.66	11.09	2.22	0.78	0.98	59.87
9	6320	340	725	104	39.6	19.4	99.7	105.0	45.8	73.7	99.9	104.1	54.6	27.2	26.9	3.02	9.96	10.32	2.81	0.48	0.95	50.43
10	3780	320	263	82	66.8	22.8	102.1	106.2	69.5	82.5	97.5	104.2	71.8	47.9	50.8	6.02	11.02	11.31	5.98	0.17	0.95	44.80
11	5660	440	1405	150	30.2	20.9	108.3	115.5	41.3	73.3	111.4	114.0	50.8	23.6	22.3	2.61	13.18	13.79	2.01	1.43	0.94	65.84
12	6280	440	1399	147	30.6	21.3	108.8	116.1	41.5	75.5	112.5	115.1	52.1	24.0	22.8	2.63	12.84	13.44	2.03	1.42	0.94	65.93
13	7100	440	1389	146	30.8	21.4	109.9	117.2	41.8	78.1	113.8	116.5	53.6	24.2	22.9	2.65	12.41	12.95	2.05	1.42	0.94	65.94
14	6822	440	1283	142	37.5	22.5	109.1	116.0	45.9	79.1	112.9	115.3	57.2	27.1	26.1	3.03	12.49	13.04	2.54	0.86	0.95	65.76
15	6334	460	1153	148	46.5	23.4	108.8	115.7	53.5	77.4	109.2	111.7	61.3	32.9	32.4	3.83	13.10	13.70	3.43	0.55	0.94	67.99
16	6340	460	751	137	56.7	24.6	110.0	116.4	62.8	86.9	110.8	114.3	70.6	40.0	40.3	5.01	13.12	13.69	4.73	0.37	0.95	66.99
17	5640	460	291	125	68.4	25.6	111.0	116.8	74.3	92.4	108.2	112.6	79.3	50.2	51.6	6.82	13.53	13.98	6.63	0.26	0.94	65.42
18	7960	460	554	135	53.6	24.2	112.2	118.7	60.0	93.9	113.8	117.9	71.4	36.8	36.8	4.62	12.42	12.99	4.33	0.43	0.95	67.34
19	7820	460	849	141	48.7	23.8	111.5	118.2	55.5	89.1	114.0	117.4	67.1	33.8	33.4	4.06	12.45	13.04	3.65	0.52	0.96	67.68
20	7920	460	1107	147	42.0	23.4	110.1	117.0	49.7	83.7	113.3	116.0	61.7	30.0	29.3	3.41	12.41	13.03	2.92	0.71	0.96	68.37
21	4380	380	1112	129	39.1	23.3	111.4	117.3	45.5	78.1	113.1	116.4	56.6	28.8	27.9	3.00	12.83	13.30	2.69	0.69	0.95	55.72
22	4800	380	1039	125	44.2	23.6	110.8	116.6	50.4	80.3	112.5	115.7	60.2	31.6	31.1	3.49	12.46	12.90	3.23	0.52	0.95	55.68
23	4420	380	883	121	50.8	23.9	111.3	116.8	56.7	82.9	112.0	115.9	65.1	36.5	36.8	4.21	12.77	13.19	4.01	0.38	0.95	55.11
24	3100	380	660	113	61.7	25.5	113.3	118.3	66.9	85.7	111.6	115.8	72.1	46.0	47.3	5.60	14.10	14.31	5.49	0.26	0.97	53.41
25	2960	320	730	102	53.0	24.8	113.7	118.3	57.8	82.4	112.3	117.4	64.4	39.7	40.3	4.34	13.14	13.44	4.24	0.29	0.93	44.78
26	2980	320	852	109	43.4	23.8	113.1	117.9	48.9	78.5	112.6	116.9	58.1	33.2	33.0	3.33	13.20	13.49	3.18	0.45	0.94	45.38
27	3090	320	917	111	38.7	23.4	112.1	117.1	44.3	76.2	112.0	116.1	54.6	30.0	29.4	2.89	12.98	13.30	2.69	0.59	0.94	45.92
28	2960	320	944	108	28.8	22.2	110.5	115.6	40.3	71.8	109.8	114.4	47.4	24.9	23.6	2.21	13.01	13.48	1.90	1.43	0.95	46.16
29	6900	250	446	70	31.0	21.1	91.1	95.3	37.4	67.2	88.4	94.6	45.2	23.8	22.9	2.25	7.12	7.51	2.10	0.75	0.92	36.88
30	6140	260	352	70	40.2	22.0	89.4	93.4	45.4	69.0	87.0	92.8	51.5	28.9	29.1	2.99	7.62	7.92	2.91	0.41	0.95	38.27
31	5060	260	244	68	49.4	22.7	90.7	94.5	54.3	72.4	87.1	93.5	58.2	36.3	37.8	3.92	8.19	8.48	3.87	0.26	0.94	37.59
32	3940	240	150	59	56.8	24.1	91.9	95.3	61.1	74.4	86.1	93.8	62.3	42.2	44.7	4.78	8.45	8.67	4.78	0.18	0.92	34.04
33	2620	200	66	50	65.6	24.4	92.1	94.8	67.3	76.1	84.4	93.9	63.4	47.9	52.1	5.66	8.41	8.58	5.66	0.11	0.94	27.04
34	2240	140	63	39	57.7	24.1	87.7	89.7	58.7	69.2	77.4	88.8	50.5	41.3	45.1	4.45	6.51	6.58	4.45	0.10	0.93	18.69
35	1400	140	141	40	56.6	24.3	89.1	91.0	57.2	62.8	79.5	90.1	50.1	40.8	44.4	4.26	7.79	7.90	4.26	0.10	0.93	18.30
36	1380	120	176	43	42.9	23.4	89.2	90.9	50.6	59.3	79.3	89.9	43.2	36.9	38.4	3.10	6.85	6.89	3.10	0.15	0.93	15.22
37	1360	120	204	46	36.3	22.7	89.6	91.4	46.6	56.6	79.6	90.4	38.0	30.8	31.5	2.52	6.82	6.90	2.52	0.22	0.93	15.28
38	1440	120	216	45	30.1	21.9	89.6	91.4	44.0	54.8	79.4	90.5	34.1	26.3	25.9	2.05	6.63	6.72	2.05	0.38	0.95	15.31
39	1500	120	246	44	23.9	21.2	89.3	91.2	42.7	52.4	79.2	90.1	31.4	24.5	23.5	1.66	6.35	6.47	1.65	1.15	0.93	15.24
40	5300	220	540	57	25.5	21.0	88.3	91.9	35.7	58.6	85.4	91.2	38.7	22.5	21.3	1.85	6.81	7.14	1.77	1.44	0.95	32.00
41	6060	220	481	57	25.5	20.9	87.4	91.0	36.7	60.3	84.5	90.3	39.2	22.5	21.4	1.85	6.46	6.81	1.76	1.44	0.96	32.10
42	4020	220	554	60	25.4	20.9	86.1	89.7	32.7	53.7	82.6	87.9	37.4	22.6	21.4	1.83	7.33	7.53	1.73	1.44	0.96	31.92
43	4960	220	479	61	31.1	21.6	84.9	88.5	35.0	57.5	82.3	87.7	41.0	24.2	23.3	2.12	6.92	7.17	2.06	0.68	0.95	32.06
44	3540	220	452	62	32.1	21.7	84.5	88.0	36.2	51.7	77.4	82.8	40.7	25.5	24.9	2.21	7.39	7.66	2.20	0.59	0.96	31.80
45	2940	180	331	50	37.6	22.5	86.3	89.1	41.9	58.9	81.2	88.3	44.1	29.5	30.2	2.67	7.01	7.19	2.67	0.32	0.95	25.23

Table A.7: Reconciliated measurements gathered on the test rig ORC_2

$Point\#$ [−]	N_{pp} [rpm]	$\dot{W}_{exp}$ [W]	$\dot{W}_{pp}$ [W]	$T_{htf,c,ex}$ [°C]	$T_{htf,c,su}$ [°C]	$T_{htf,h,ex}$ [°C]	$T_{htf,h,su}$ [°C]	$T_{sub,su}$ [°C]	$T_{cd,su}$ [°C]	$T_{exp,ex}$ [°C]	$T_{exp,su}$ [°C]	$T_{ev,ex}$ [°C]	$T_{ev,su}$ [°C]	$T_{pre,su}$ [°C]	$T_{pp,ex}$ [°C]	$T_{pp,su}$ [°C]	$P_{htf,c}$ [bar]	$P_{htf,h}$ [bar]	$P_{exp,ex}$ [bar]	$P_{exp,su}$ [bar]	$P_{pp,ex}$ [bar]	$P_{pp,su}$ [bar]	$\dot{m}_{htf,c}$ [kg/s]	$\dot{m}_{htf,h}$ [kg/s]	$\dot{m}_{wf}$ [g/s]
1	243	1134	258	50.4	30.6	75.9	150.5	61.6	61.6	86.3	101.1	102.9	83.6	53.8	35.5	35.0	2.26	10.89	3.36	8.68	9.80	2.67	0.74	0.19	277.08
2	274	2182	314	53.2	32.2	85.2	151.8	67.1	67.1	95.0	113.4	115.4	92.6	57.9	37.2	36.6	2.37	10.22	3.62	10.08	11.46	2.90	0.80	0.24	309.93
3	291	2073	335	53.9	33.2	84.5	151.4	66.8	66.8	93.1	110.9	113.1	91.8	58.0	38.6	38.0	2.42	11.13	3.71	10.18	11.62	2.91	0.84	0.25	328.73
4	331	3557	423	53.4	31.0	89.3	152.4	67.1	67.1	95.3	117.2	119.8	96.3	57.8	36.9	36.3	2.29	11.75	3.63	11.58	13.37	2.81	0.89	0.31	371.74
5	311	3454	387	54.0	32.6	91.1	152.8	71.3	71.3	101.3	123.0	125.2	98.0	60.2	37.9	37.3	2.37	11.75	3.66	11.30	12.95	2.99	0.90	0.30	350.30
6	405	4641	581	58.7	34.9	97.7	154.5	71.9	71.9	100.9	124.7	128.2	103.7	62.8	41.2	40.5	2.54	11.06	4.23	13.80	16.21	3.30	1.02	0.41	453.86
7	407	4588	590	55.8	32.1	94.2	154.1	67.2	67.2	95.6	119.8	123.6	100.5	59.6	38.4	37.7	2.34	9.52	3.93	13.49	15.94	2.95	1.02	0.39	454.15
8	447	5755	649	58.2	34.0	100.7	154.8	67.7	67.7	98.2	125.7	129.9	106.7	62.3	39.6	38.9	2.45	11.11	4.23	15.15	17.96	3.19	1.08	0.47	496.27
9	508	6889	902	59.5	35.3	104.9	156.8	68.9	68.9	100.0	129.9	135.2	110.4	64.4	41.1	40.3	2.47	11.03	4.44	16.95	20.48	3.22	1.21	0.55	559.29
10	486	6614	829	58.8	35.4	102.9	157.0	68.7	68.7	99.3	128.6	133.4	108.7	63.6	40.7	39.9	2.47	11.17	4.31	16.34	19.57	3.39	1.21	0.51	539.00
11	323	2260	373	55.6	37.5	85.1	160.7	71.5	71.5	96.3	114.4	117.0	92.5	60.9	42.5	42.0	2.53	12.78	3.89	11.11	12.84	3.20	1.07	0.24	364.20
12	372	3312	440	58.1	39.5	90.8	161.2	72.8	72.8	97.6	118.7	122.0	97.9	62.9	44.5	43.9	2.66	9.19	4.20	12.74	14.91	3.43	1.17	0.30	416.59
13	386	4648	541	56.8	35.7	95.0	157.0	72.2	72.2	99.3	123.9	127.0	101.6	61.1	41.0	40.2	2.48	11.04	4.01	13.36	15.46	3.16	1.09	0.36	432.24
14	479	5831	546	61.9	40.7	97.6	168.2	76.3	76.3	102.8	129.2	133.7	103.8	65.8	46.0	45.4	2.70	11.04	4.66	15.88	18.95	3.57	1.30	0.38	529.00
15	478	5502	545	62.9	41.9	97.8	167.8	77.1	77.1	103.3	128.7	133.3	104.0	66.9	47.2	46.7	2.77	10.26	4.79	15.75	18.86	3.76	1.31	0.38	528.72
16	525	5421	581	63.8	42.3	96.7	167.3	71.2	71.2	96.2	122.9	128.8	102.8	66.6	47.9	47.4	2.81	10.02	5.01	16.44	20.05	3.71	1.35	0.40	578.87
17	525	5415	583	63.2	42.5	96.3	166.8	70.6	70.6	95.0	121.9	127.9	102.5	66.3	48.0	47.5	2.81	9.92	4.95	16.36	19.93	3.67	1.40	0.40	578.95
18	527	6072	671	63.7	42.5	100.5	166.8	74.5	74.5	100.3	128.0	133.5	106.6	67.4	48.0	47.4	2.83	9.90	5.00	16.93	20.52	3.67	1.40	0.43	578.94
19	449	4513	587	63.4	42.9	98.4	164.9	78.9	78.9	105.0	128.2	132.2	104.6	67.8	48.3	47.6	2.86	9.94	4.84	15.03	17.83	3.74	1.26	0.38	497.98
20	399	3609	516	62.9	42.1	96.1	165.1	79.4	79.4	106.3	127.3	130.7	102.4	67.7	47.6	46.9	2.83	10.33	4.76	13.90	16.36	3.95	1.13	0.33	446.44
21	397	3248	521	64.4	42.0	96.3	164.8	80.0	80.0	107.2	127.0	130.5	102.5	68.3	47.9	47.3	2.88	10.38	4.96	13.87	16.34	4.25	1.05	0.33	446.15
22	488	5641	775	62.6	38.7	95.1	169.2	77.9	77.9	101.4	127.6	130.2	101.8	62.1	44.4	43.6	2.67	10.33	4.78	16.02	17.76	3.77	1.22	0.38	547.65
23	517	5953	854	63.7	40.5	97.2	169.2	78.8	78.8	101.8	128.7	131.6	103.7	63.6	46.2	45.3	2.73	10.19	5.02	16.77	18.71	3.92	1.32	0.41	578.32
24	516	6047	855	62.7	39.4	96.8	169.0	78.1	78.1	101.3	128.5	131.5	103.3	62.7	45.2	44.4	2.61	10.12	4.90	16.75	18.73	3.92	1.31	0.41	578.46
25	517	6225	856	63.1	40.1	96.1	168.7	75.4	75.4	97.9	126.1	129.3	102.7	62.5	45.5	44.7	2.64	10.06	5.00	16.89	18.90	3.96	1.31	0.40	579.48
26	519	6431	870	63.3	39.9	98.8	168.5	77.4	77.4	100.9	129.5	132.5	105.4	63.0	45.2	44.4	2.65	9.97	5.03	17.30	19.31	3.86	1.31	0.43	579.42
27	520	6632	871	62.0	38.4	98.0	168.0	76.2	76.2	99.9	128.9	132.0	104.6	61.7	43.8	42.9	2.55	9.90	4.88	17.22	19.25	3.63	1.31	0.43	579.93
28	519	6820	884	62.8	39.0	100.8	167.8	79.3	79.3	103.8	132.7	135.7	107.3	63.0	44.4	43.6	2.61	9.84	4.97	17.55	19.60	3.80	1.31	0.45	579.49
29	519	6750	878	62.8	40.7	101.2	167.5	80.4	80.4	104.3	132.9	135.8	107.6	64.0	45.9	45.1	2.70	9.81	5.02	17.52	19.55	4.00	1.40	0.45	580.01
30	442	4850	543	63.7	40.0	96.0	165.2	80.7	80.7	102.5	126.9	129.0	102.6	61.6	45.1	44.5	2.71	9.74	4.84	15.13	16.60	3.91	1.12	0.37	498.26
31	470	5245	730	63.4	41.0	104.1	152.1	81.7	81.7	102.8	127.8	130.2	109.3	62.2	46.3	45.5	2.64	6.85	4.88	15.73	17.36	4.03	1.27	0.57	528.02
32	315	1787	339	60.4	39.6	90.9	149.9	78.7	78.7	99.1	115.4	116.9	90.7	59.8	44.5	43.9	2.66	6.80	4.41	11.24	12.28	3.81	0.93	0.31	359.10
33	350	2393	392	62.5	39.5	95.1	150.0	80.9	80.9	102.2	120.0	121.7	94.8	61.2	45.1	44.5	2.70	6.78	4.65	12.28	13.41	3.99	0.93	0.37	397.82
34	387	3477	461	62.8	41.0	98.3	149.9	82.1	82.1	104.0	124.6	126.4	104.2	62.2	45.8	45.2	2.71	6.77	4.69	13.50	14.77	3.94	1.08	0.44	437.32
35	416	4549	518	62.7	40.9	102.7	150.4	83.7	83.7	106.4	129.6	131.6	108.1	62.7	45.6	45.0	2.69	6.76	4.67	14.55	16.00	3.90	1.17	0.52	468.26
36	500	5829	608	62.9	40.1	106.4	151.0	81.3	81.3	102.7	129.0	131.5	111.5	61.6	45.5	44.9	2.63	6.75	4.85	16.38	18.06	3.72	1.31	0.65	557.90
37	262	1364	251	55.1	34.5	85.0	141.9	71.9	71.9	92.5	107.8	109.0	83.8	53.7	38.3	37.8	2.34	6.21	3.80	9.61	10.39	3.19	0.79	0.27	300.16
38	312	2358	330	57.5	36.5	92.2	142.7	78.3	78.3	99.7	117.7	119.1	90.3	57.5	41.4	40.9	2.52	6.20	4.03	11.09	12.03	3.53	0.93	0.37	356.41
39	367	3569	462	60.0	38.1	98.2	143.6	79.8	79.8	101.2	122.1	123.8	97.1	58.9	42.8	42.2	2.58	6.19	4.33	12.87	14.05	3.60	1.04	0.48	416.40
40	422	4890	574	61.1	36.9	102.9	144.0	80.2	80.2	102.6	126.7	128.7	107.8	59.1	42.2	41.5	2.52	6.18	4.44	14.45	15.85	3.58	1.08	0.62	476.39
41	478	5838	657	62.1	39.1	108.6	144.7	82.3	82.3	104.3	130.4	132.6	112.8	61.0	44.4	43.7	2.62	6.19	4.69	15.95	17.53	3.78	1.27	0.79	536.82
42	528	6669	882	61.7	39.2	112.0	144.6	78.3	78.3	98.9	128.3	131.1	115.3	60.0	44.4	43.6	2.57	6.18	4.88	17.44	19.22	3.68	1.40	0.94	589.60
43	555	6856	939	62.9	39.6	113.3	144.5	78.2	78.2	98.6	128.4	131.4	116.4	60.5	45.1	44.2	2.61	6.17	5.05	17.90	19.78	3.67	1.41	1.02	618.65
44	462	5617	586	61.5	39.1	110.9	136.7	82.1	82.1	101.9	127.9	130.1	113.4	58.9	44.0	43.4	2.62	5.36	4.65	15.65	17.14	3.71	1.27	1.07	519.12

Appendix B.2. Polynomial regression models

– Pump model:

$$\varepsilon_{is,pp} = \sum_{i=0}^{2}\sum_{j=0}^{2} a_{ij}(N_{pp})^{i}(r_p)^{j} \tag{B.8}$$

$$\varepsilon_{vol,pp} = \sum_{i=0}^{2}\sum_{j=0}^{2} b_{ij}(N_{pp})^{i}(r_p)^{j} \tag{B.9}$$

$$\dot{W}_{mec,pp} = \dot{m}_{pp}(h_{ex,pp} - h_{su,pp}) + AU_{loss}(\bar{T}_{pp} - T_{amb}) \tag{B.10}$$

– Expander model:

$$\varepsilon_{is,exp} = \sum_{i=0}^{2}\sum_{j=0}^{2}\sum_{k=0}^{2} c_{ijk}(\rho_{su,exp})^{i}(r_p)^{j}(N_{exp})^{k} \tag{B.11}$$

$$\varepsilon_{vol,exp} = \sum_{i=0}^{2}\sum_{j=0}^{2}\sum_{k=0}^{2} d_{ijk}(\rho_{su,exp})^{i}(r_p)^{j}(N_{exp})^{k} \tag{B.12}$$

$$\dot{m}_{exp}(h_{su,exp} - h_{ex,exp}) = \dot{W}_{mec,exp} + AU_{loss}(\bar{T}_{exp} - T_{amb}) \tag{B.13}$$

– Heat exchanger model:

$$\varepsilon_{th} = \sum_{i=0}^{2}\sum_{j=0}^{2} e_{ij}(\dot{m}_{h,su})^{i}(\dot{m}_{c,su})^{j} \tag{B.14}$$

865 *Appendix B.3. Semi-empirical models*

– Pump model:

$$\dot{m}_{pp} = \underbrace{(\rho_{su,pp}N_{pp}V_{dis,pp})}_{\dot{m}_{ideal,pp}} - \underbrace{(A_{lk}\sqrt{2\rho_{su,pp}(P_{ex,pp} - P_{su,pp})})}_{\dot{m}_{lk,pp}} \tag{B.15}$$

$$\dot{W}_{mec,pp} = \underbrace{(\dot{W}_{loss} + K_{loss}\dot{V}_{su,pp}(P_{pp,ex} - P_{pp,su}))}_{\dot{W}_{loss,pp}} + \underbrace{(\dot{V}_{su,pp}(P_{pp,ex} - P_{pp,su}))}_{\dot{W}_{is,pp}} \tag{B.16}$$

$$\dot{W}_{mec,pp} = \dot{m}_{pp}(h_{ex,pp} - h_{su,pp}) + AU_{loss}(\bar{T}_{pp} - T_{amb}) \tag{B.17}$$

– Expander model: please refer to [31] for a detailed description of the expander model.

– Heat exchanger model:

$$\dot{Q}_i = A_i U_i \Delta T_{log,i} \tag{B.18}$$

$$U_i = \left(\frac{1}{\alpha_{conv,h,i}} + \frac{1}{\alpha_{conv,c,i}} \right)^{-1} \tag{B.19}$$

$$\sum_{i=0}^{N} A_i = A_{HEX} \tag{B.20}$$

$$\alpha_{conv} = \alpha_{conv,nom} \left(\frac{\dot{m}}{\dot{m}_{nom}} \right)^{n} \tag{B.21}$$

Appendix B.4. Pipeline losses

– Pressure losses:

$$\Delta P = K \varphi_{su} + B \tag{B.22}$$

$$\varphi_{su} = \frac{\dot{m}^2}{\rho_{su}} \tag{B.23}$$

– Heat losses:

$$\dot{Q}_{loss} = AU_{loss}(T_{su} - T_{amb}) \tag{B.24}$$

Appendix C. Detailed results of the study

870 Detailed values of RMSEs and MAPES computed for both the component-level and the cycle-level analyses are summarized in Table C.8 and C.9.

Table C.8: Global results - RMSE (units : same than the variables)

			ORC 1							ORC 2									
			$\dot{Q}_{ev,1}$	$\dot{Q}_{rec,1}$	$\dot{Q}_{cd,1}$	$\dot{W}_{pp,1}$	$\dot{W}_{exp,1}$	$\dot{m}_{pp,1}$	$\dot{m}_{exp,1}$	$\dot{Q}_{ev,2}$	$\dot{Q}_{rec,2}$	$\dot{Q}_{cd,2}$	$\dot{Q}_{sub,2}$	$\dot{Q}_{pre,2}$	$\dot{W}_{pp,2}$	$\dot{W}_{exp,2}$	$\dot{m}_{pp,2}$	$\dot{m}_{exp,2}$
Component-level analysis	Fitting	CstEff model	87	219	347	29	238	1.59e-03	1.53e-02	1923	1561	3258	472	2187	102	565	4.40e-03	7.11e-03
		PolEff model	68	89	125	8	54	5.63e-04	1.15e-03	1541	1550	1885	451	1340	72	136	3.13e-04	4.67e-03
		SemiEmp model	77	73	151	5	49	8.01e-04	1.61e-03	1062	1560	818	382	979	87	205	5.82e-03	7.27e-03
	Extrap	CstEff model	126	231	338	36	248	1.76e-03	1.22e-02	1754	1780	3980	681	3191	84	612	6.07e-03	8.89e-03
		PolEff model	129	142	97	12	147	1.27e-03	1.48e-03	2230	2053	2842	662	6833	97	466	5.80e-04	1.72e-02
		SemiEmp model	119	74	158	7	48	9.80e-04	1.67e-03	1236	1883	1044	449	1384	85	229	7.47e-03	9.06e-03
Cycle-level analysis	Fitting	CstEff model	320	133	260	23	190	1.64e-03	1.64e-03	4842	2322	3540	3419	4343	80	632	4.30e-03	4.30e-03
		PolEff model	147	93	136	9	75	5.72e-04	5.72e-04	5276	2189	2871	3202	3115	281	1311	5.13e-03	5.13e-03
		SemiEmp model	150	83	129	6	57	6.99e-04	6.99e-04	2118	2194	3405	2915	1206	79	365	6.16e-03	6.16e-03
	Extrap	CstEff model	441	91	337	19	207	1.53e-03	1.53e-03	4116	2665	5236	4040	2877	88	666	6.24e-03	6.24e-03
		PolEff model	153	402	151	19	94	6.80e-04	6.80e-04	5821	2954	15334	14696	5601	201	422	2.63e-03	2.63e-03
		SemiEmp model	155	137	127	7	67	8.36e-04	8.36e-04	1637	2870	6177	4136	1452	102	392	7.95e-03	7.95e-03

Table C.9: Global results - MAPE (units : %)

			ORC 1							ORC 2									
			$\dot{Q}_{ev,1}$	$\dot{Q}_{rec,1}$	$\dot{Q}_{cd,1}$	$\dot{W}_{pp,1}$	$\dot{W}_{exp,1}$	$\dot{m}_{pp,1}$	$\dot{m}_{exp,1}$	$\dot{Q}_{ev,2}$	$\dot{Q}_{rec,2}$	$\dot{Q}_{cd,2}$	$\dot{Q}_{sub,2}$	$\dot{Q}_{pre,2}$	$\dot{W}_{pp,2}$	$\dot{W}_{exp,2}$	$\dot{m}_{pp,2}$	$\dot{m}_{exp,2}$
Component-level analysis	Fitting	CstEff model	0.52	18.56	3.13	26.71	32.51	3.52	24.67	2.10	11.73	2.56	2.84	6.15	13.23	14.64	0.73	1.20
		PolEff model	0.44	5.93	1.42	8.18	9.34	1.30	2.00	1.70	11.38	1.11	2.87	3.58	8.65	2.68	0.05	0.81
		SemiEmp model	0.51	11.24	1.84	4.89	9.36	2.30	3.90	1.19	10.44	0.81	4.39	2.10	9.66	4.33	1.12	1.17
	Extrapolation	CstEff model	0.65	26.28	3.00	35.86	40.45	4.87	28.89	2.00	13.28	2.77	3.69	8.34	15.12	21.76	1.10	1.51
		PolEff model	0.73	8.20	1.40	12.83	21.29	2.14	4.52	2.37	14.25	1.92	4.01	9.12	14.66	9.42	0.08	3.05
		SemiEmp model	0.65	16.11	1.69	5.51	12.03	3.11	3.77	1.59	13.07	0.82	4.98	4.00	10.80	5.52	1.60	1.54
Cycle-level analysis	Fitting	CstEff model	2.90	14.40	2.80	25.14	26.26	3.68	3.68	4.31	16.61	3.44	26.31	8.95	12.03	13.94	0.71	0.71
		PolEff model	1.53	6.91	1.54	9.40	10.70	1.29	1.29	4.13	15.11	2.66	23.57	7.26	20.06	11.18	0.54	0.54
		SemiEmp model	1.88	13.89	1.77	6.99	8.12	2.03	2.03	2.10	14.23	3.49	25.29	3.92	9.73	7.09	1.16	1.16
	Extrapolation	CstEff model	3.81	14.07	3.43	21.06	34.60	4.47	4.47	4.57	20.05	5.28	41.38	8.25	17.18	17.95	0.99	0.99
		PolEff model	1.91	27.63	2.01	22.88	13.15	2.30	2.30	5.81	22.70	13.58	165.71	15.30	36.52	8.12	0.45	0.45
		SemiEmp model	2.23	32.80	2.06	8.37	11.32	3.01	3.01	1.72	19.35	5.52	40.63	4.47	14.72	8.97	1.56	1.56

Highlights:

- Three methods are compared to simulate the off-design operation of ORC engines;
- Post-processed experimental measurements are used as reference database;
- Fitting and extrapolation capabilities of these 3 modelling paradigms are studied;
- Both component-level and system-level analyses are performed;
- Semi-empirical models demonstrate to be the best modelling approach.

ACCEPTED MANUSCRIPT